Earth's Future

RESEARCH ARTICLE
10.1029/2020EF001616

Projecting Exposure to Extreme Climate Impact Events Across Six Event Categories and Three Spatial Scales

Stefan Lange[1], Jan Volkholz[1], Tobias Geiger[1,2], Fang Zhao[3], Iliusi Vega[1], Ted Veldkamp[4,5], Christopher P. O. Reyer[1], Lila Warszawski[1], Veronika Huber[6], Jonas Jägermeyr[1,7,8], Jacob Schewe[1], David N. Bresch[9,10], Matthias Büchner[1], Jinfeng Chang[5,11], Philippe Ciais[11], Marie Dury[12], Kerry Emanuel[13], Christian Folberth[5], Dieter Gerten[1,14], Simon N. Gosling[15], Manolis Grillakis[16], Naota Hanasaki[17], Alexandra-Jane Henrot[12], Thomas Hickler[18,19], Yasushi Honda[20], Akihiko Ito[17], Nikolay Khabarov[5], Aristeidis Koutroulis[21], Wenfeng Liu[11,22], Christoph Müller[1], Kazuya Nishina[17], Sebastian Ostberg[1], Hannes Müller Schmied[18,19], Sonia I. Seneviratne[23], Tobias Stacke[24], Jörg Steinkamp[19,25], Wim Thiery[23,26], Yoshihide Wada[5], Sven Willner[1], Hong Yang[22,27], Minoru Yoshikawa[28], Chao Yue[11,29], and Katja Frieler[1]

[1]Potsdam Institute for Climate Impact Research (PIK), Member of the Leibniz Association, Potsdam, Germany, [2]Climate and Environment Consultancy, Deutscher Wetterdienst (DWD), Stahnsdorf, Germany, [3]School of Geographic Sciences, East China Normal University, Shanghai, China, [4]Institute for Environmental Studies, Vrije Universiteit Amsterdam, Amsterdam, Netherlands, [5]International Institute for Applied Systems Analysis (IIASA), Laxenburg, Austria, [6]Department of Physical, Chemical, and Natural Systems, Universidad Pablo de Olavide, Sevilla, Spain, [7]NASA Goddard Institute for Space Studies, New York, NY, USA, [8]Department of Computer Science, University of Chicago, Chicago, IL, USA, [9]Institute for Environmental Decisions, ETH Zurich, Zurich, Switzerland, [10]Federal Office of Meteorology and Climatology MeteoSwiss, Zurich, Switzerland, [11]Laboratoire des Sciences du Climat et de l'Environnement, CEA CNRS UVSQ, Institut Pierre Simon Laplace, Gif sur Yvette, France, [12]Unit for Modeling of Climate and Biogeochemical Cycles, University of Liège, Liège, Belgium, [13]Lorenz Center, Massachusetts Institute of Technology, Cambridge, MA, USA, [14]Geography Department, Humboldt University of Berlin, Berlin, Germany, [15]School of Geography, University of Nottingham, Nottingham, UK, [16]Lab of Geophysical-Remote Sensing and Archaeo-environment, Institute for Mediterranean Studies, Rethymno, Greece, [17]National Institute for Environmental Studies, Tsukuba, Japan, [18]Institute of Physical Geography, Goethe University Frankfurt, Frankfurt, Germany, [19]Senckenberg Leibniz Biodiversity and Climate Research Centre (SBiK-F), Frankfurt, Germany, [20]Faculty of Health and Sport Sciences, University of Tsukuba, Tsukuba, Japan, [21]School of Environmental Engineering, Technical University of Crete, Chania, Greece, [22]Swiss Federal Institute of Aquatic Science and Technology (Eawag), Dübendorf, Switzerland, [23]Institute for Atmospheric and Climate Science, ETH Zurich, Zurich, Switzerland, [24]Institute of Coastal Research, Helmholtz-Zentrum Geesthacht, Geesthacht, Germany, [25]Zentrum für Datenverarbeitung, Johannes Gutenberg-Universität Mainz, Mainz, Germany, [26]Department of Hydrology and Hydraulic Engineering, Vrije Universiteit Brussel, Brussels, Belgium, [27]Department of Environmental Sciences, MUG, University of Basel, Basel, Switzerland, [28]Mizuho Information and Research Institute Inc., Tokyo, Japan, [29]State Key Laboratory of Soil Erosion and Dryland Farming on the Loess Plateau, Northwest A&F University, Yangling, Shaanxi, China

Key Points:
- We quantify the pure effect of climate change on the exposure to extreme climate impact events, for both historical and future time periods
- Global warming increases the global population exposure to river floods, tropical cyclones, crop failure, wildfires, droughts, and heatwaves
- The largest increases in exposure are projected for tropical and subtropical regions

Supporting Information:
- Supporting Information S1

Correspondence to:
S. Lange and K. Frieler,
slange@pik-potsdam.de;
katja.frieler@pik-potsdam.de

Citation:
Lange, S., Volkholz, J., Geiger, T., Zhao, F., Vega, I., Veldkamp, T., et al. (2020). Projecting exposure to extreme climate impact events across six event categories and three spatial scales. *Earth's Future*, *11*, e2020EF001616. https://doi.org/10.1029/2020EF001616

Received 15 MAY 2020
Accepted 21 OCT 2020
Accepted article online 13 NOV 2020

Abstract The extent and impact of climate-related extreme events depend on the underlying meteorological, hydrological, or climatological drivers as well as on human factors such as land use or population density. Here we quantify the pure effect of historical and future climate change on the exposure of land and population to extreme climate impact events using an unprecedentedly large ensemble of harmonized climate impact simulations from the Inter-Sectoral Impact Model Intercomparison Project phase 2b. Our results indicate that global warming has already more than doubled both the global land area and the global population annually exposed to all six categories of extreme events considered: river floods, tropical cyclones, crop failure, wildfires, droughts, and heatwaves. Global warming of 2°C relative to preindustrial conditions is projected to lead to a more than fivefold increase in cross-category aggregate exposure globally. Changes in exposure are unevenly distributed, with tropical and subtropical regions facing larger increases than higher latitudes. The largest increases in overall exposure are projected for the population of South Asia.

Plain Language Summary Global warming changes the frequency, intensity, and spatial distribution of extreme events. We analyze computer simulations of river floods, tropical cyclones, crop failure, wildfires, droughts, and heatwaves under past, present-day, and potential future climate conditions.

Our results show that global warming increases the number of people around the world that are affected by these events each year, both for all event types combined and each type individually. Changes in the chance of being affected by extreme events are unevenly distributed in space. Particularly large increases are simulated for tropical and subtropical regions.

1. Introduction

From 1980 to 2018, around 400 weather-related disasters annually have caused around 23,000 fatalities and US$ 100 billion worth of direct economic damages worldwide each year (Munich RE, 2020). Weather events have also been the dominant driver of internal displacement, with an annual average of 23 million newly displaced people from 2009 to 2019 (IDMC, 2020). Moreover, these events push people into poverty and prevent poor people from escaping poverty (Hallegatte et al., 2015), and they have the potential to dampen long-term economic growth (Hsiang & Jina, 2014; Kousky, 2014).

Multiple categories of events contributed to these damages. For 1980 to 2018, Munich RE (2020) attributes 55% of the direct economic losses caused by weather-related disasters to storms, 27% to floods, and 18% to extreme temperatures, droughts, and wildfires. While these events are often referred to as *natural* disasters, the underlying extreme weather patterns have already started to show a marked signal of *anthropogenic* forcing (Coumou & Rahmstorf, 2012; Hoegh-Guldberg et al., 2018; Lehmann et al., 2015; Trenberth et al., 2015). Continuing global warming is projected to further change the events' frequency, intensity, and spatial distribution (Dai, 2013; Hirabayashi et al., 2013; Im et al., 2017; Pechony & Shindell, 2010; Sobel et al., 2016).

In addition to the severity of the event, the amount of damage inflicted by an extreme weather event depends on a wide range of socioeconomic factors including patterns of land use, water, forest and agricultural management. It also depends on the extent to which people and economic assets are exposed to the event (Andela et al., 2017; Geiger et al., 2016; Geiger & Stomper, 2020; Winsemius et al., 2013). This renders the detection of a climate change signal in historical variations of observed impacts of weather-related disasters difficult, except in those regions where direct human influences are low (Abatzoglou & Williams, 2016), or to cases in which the effect of climate change can be empirically separated from the effects of other drivers (Lobell et al., 2011).

Process-based climate impact models allow for such a separation, since individual drivers can be systematically isolated and their contributions to changes in impacts quantified using a suitable portfolio of simulation scenarios (Frieler et al., 2017). These models represent physical and biogeochemical processes, such as evapotranspiration (e.g., in hydrological models) and photosynthesis (e.g., in vegetation models). Using projections of climate change and socioeconomic change as input, the models can be used to project and assess the associated impacts and risks (Piontek et al., 2014; Rosenzweig et al., 2017). While a targeted scenario portfolio allows for quantification of the effects of different drivers, the modeling uncertainty of such projections can be quantified in a multimodel framework, where harmonized inputs and a common modeling protocol are used for simulations with multiple models from the same sector (e.g., multiple hydrological models). To allow for a consistent multisectoral risk assessment, multimodel frameworks are extended to cover models from multiple sectors (e.g., multiple hydrological models and multiple vegetation models).

Phase 2b of the Inter-Sectoral Impact Model Intercomparison Project (ISIMIP2b) resulted in a particularly large database of process-based climate-impact-model output produced in a multisectoral, multimodel framework. To our knowledge, it is the largest database of its kind currently available. All model simulations are based on the same climate and socioeconomic input data and follow the simulation protocol described in Frieler et al. (2017). Here we make use of this database to quantify the pure effect of climate change on both the land area and population annually exposed to extreme climate impact events in today's 1°C warmer world as well as at higher levels of global warming relative to preindustrial conditions. The effects of historical and future climate change are quantified by comparing with baseline simulations that combine preindustrial climate conditions with historically varying and fixed present-day socioeconomic conditions, respectively.

Our analysis covers six important event categories, namely river floods, tropical cyclones, wildfires, crop failure, droughts, and heatwaves. For every event category, we define a certain event magnitude and then scan the multimodel data to find where and how often this event magnitude is exceeded. These event occurrences

are then combined with land area and population patterns to quantify the exposure of land and population to extreme events. For river floods and droughts we use the output of eight hydrological models. Data for tropical cyclone projections come from a single tropical cyclone model. Wildfire projections are based on the output of five vegetation models. Crop failure is derived from the output of three crop models. Our heatwave indicator is directly computed from the climate input data used as input by the other models.

This analysis is not a complete risk assessment since we do not account for vulnerability and hence cover only two (hazard and exposure) of the three components that constitute risk according to the Intergovernmental Panel on Climate Change (IPCC; Oppenheimer et al., 2014). Nevertheless, changes in exposure are analyzed at three spatial scales. First, we study the global land area and population exposed to assess the overall direction and magnitude of change. Then we look at regional differences in projected exposure to identify hot spots of impacts of global warming. Finally, we relate changes in exposure at the national level to economic productivity to highlight distributional aspects of climate change.

2. Data and Methods

In the following we describe the impact model simulations analyzed in this study and discuss the models' fitness for purpose. We then introduce the exposure measures used and explain how we quantify the pure effect of climate change on the land area and population exposed to extreme events at different levels of global warming. Finally, we specify how we define river floods, tropical cyclones, wildfires, crop failure, droughts, and heatwaves and discuss alternatives to and limitations of these definitions.

2.1. Impact Model Simulations and Evaluation

Except for heatwaves, the exposure measures analyzed here are calculated based on process-based impact model simulations carried out within ISIMIP2b (Frieler et al., 2017). Hydrological, vegetation, and crop models were forced by bias-adjusted (Frieler et al., 2017; Lange, 2017, 2018) output of preindustrial (200 years) and historical (1861–2005) climate simulations as well as future climate projections (2006–2100) for the low emissions scenario RCP2.6 and the medium emissions scenario RCP6.0, generated with four Global Climate Models (GCMs; IPSL-CM5A-LR, HadGEM2-ES, MIROC5, and GFDL-ESM2M) within Phase 5 of the Coupled Model Intercomparison Project (CMIP5 Taylor et al., 2011). Input and output data of the impact model simulations have a spatial resolution of 0.5° latitude × 0.5° longitude. The high-resolution physical model used to generate large samples of potential realizations of tropical cyclone tracks and intensities was forced by subdaily output of the GCMs listed above.

The climate input data are restricted to four GCMs and two RCPs according to the ISIMIP2b simulation protocol. This restriction was to limit the work load of the modeling teams and thus to lower the barrier to participation in ISIMIP2b. GCM selection was heavily constrained by CMIP5 data availability, see Frieler et al. (2017) for details. Another selection criterion was equilibrium climate sensitivity (ECS). The goal was to select GCMs such that they approximately represent the CMIP5 distribution of ECS. That is why high-ECS (IPSL-CM5A-LR, HadGEM2-ES) as well as low-ESC (MIROC5, GFDL-ESM2M) models were selected. The emissions scenario selection reflects the fact that ISIMIP2b was designed to support the IPCC special report on the impacts of global warming of 1.5°C above preindustrial levels and related global greenhouse gas emission pathways. At a later stage, the high emissions scenario RCP8.5 was added to the protocol but substantially fewer simulation results are available for this than for the other two scenarios.

Exposure to river floods and droughts is calculated based on the output of eight global hydrological models (GHMs; see Table S1 in the supporting information). In particular, output of daily runoff and monthly soil moisture is used for river floods and droughts, respectively (see section 2.4 and Texts S1 and S2 for details). The ability of GHMs to simulate high-flow and low-flow conditions has been assessed in a number of model evaluation studies (Giuntoli et al., 2015; Gudmundsson et al., 2012; Huang et al., 2017; Schewe et al., 2019; Staudinger et al., 2011; Velázquez et al., 2013; Vetter et al., 2017). For high-flow conditions, this ability has been found to mainly depend on climate input data quality, whereas for low-flow conditions, GHMs usually contribute substantially to the overall modeling uncertainty, reflecting uncertainties associated with the representation of hydrological processes such as the depletion of soil moisture stores.

In addition to the eight GHMs, we use the global river model CaMa-Flood (Yamazaki et al., 2011, 2013) to calculate river flood exposure (see section 2.4). CaMa-Flood has been shown to improve the reproduction of the multimodel ensemble mean of observed peak discharge in most regions compared to the original routing

schemes used within the GHMs, although individual GHM discharge might still fit better to observations (Zhao et al., 2017) and the model is widely used to estimate global river flood risk under climate change (Dottori et al., 2018; Hirabayashi et al., 2013; Koirala et al., 2014; Pappenberger et al., 2012).

Exposure to crop failure is calculated based on maize, rice, soybean, and wheat yields simulated with three global gridded crop models (GGCMs) using ISIMIP2b land use and irrigation patterns (Frieler et al., 2017) and fixed agricultural management (Table S2). Müller et al. (2017) found that most GGCMs are capable of reproducing much of the observed temporal variability of maize, wheat, and soybean yields especially in countries with industrialized agriculture, whereas their skill in rice simulation is lower. The particular impact of heatwave and drought conditions on crop yields was studied by Schauberger et al. (2017), who found consistent responses of US maize, soybean and wheat yields to high temperatures in GGCM simulations and observations, as well as by Schewe et al. (2019), who found that GGCMs do not fully capture the extremeness of yield declines of maize and wheat that occurred in response to the 2003 European heatwave and drought.

Exposure to wildfires is derived directly from the output of burned area of five global vegetation models (GVMs; see Table S3). These models simulate a wide spread of global annual burned area values and overall they reproduce observed spatial patterns of wildfire occurrence unsatisfactorily (Text S3). These modeling uncertainties are mainly due to unrepresented or misrepresented direct human influences on wildfire ignition, suppression, and management (see Andela et al., 2017, and Text S3). Nevertheless, we interpret projected changes in burned area as a proxy for the impact of climate change on the exposure to wildfires, acknowledging that future changes in direct human influences on wildfires have the potential to reverse any of the trends found here.

Exposure to tropical cyclones is calculated based on tropical cyclone tracks generated using a dynamical tropical cyclone model (Emanuel, 2013) combined with a wind-field model (Holland, 2008) as implemented in the climate risk modeling toolbox climada (Aznar-Siguan & Bresch, 2019; Geiger et al., 2018; Gettelman et al., 2018). The dynamical downscaling approach (Emanuel et al., 2008) as well as the wind-field model have been shown to realistically reproduce observed tropical cyclone data (Geiger et al., 2018; Holland, 2008) and have been applied to project socioeconomic tropical cyclone impacts (Mendelsohn et al., 2012).

2.2. Exposure Measures

We measure exposure in a way that facilitates its comparison and aggregation across extreme event categories. This requires the use of (i) a common exposed entity and (ii) a common time scale of exposure across categories. For (i) we use the land area exposed to extreme events as the basis of our analysis because it can easily be defined for all categories considered (see section 2.4). For (ii) we use the annual time scale as this is the natural time scale for crop failure. All the other events (river floods, tropical cyclones, wildfires, droughts, and heatwaves) can theoretically hit the same location multiple times per year. To facilitate an aggregation of exposure across categories, we measure the land area that is exposed to at least one event in a given year.

In addition to land area, we measure population exposure, assuming that only people living in the exposed area can be exposed. For river floods, tropical cyclones, wildfires, and heatwaves, we assume that all people in the exposed area are exposed. For droughts we assume that only the rural population is exposed. For crop failure we assume that exposure is limited to those whose income depends on the failed crop (see Text S4). In all cases, population exposure is calculated by multiplying the total/rural/farming population of a grid cell by the exposed land area fraction of the grid cell (while extensive events are assumed to expose entire grid cells, confined events are assumed to expose only fractions of a grid cell, see section 2.4). For that purpose we use historically changing population data during 1861–2005 (Klein Goldewijk et al., 2017) and constant 1860 and 2005 population data before and after that time period, respectively. Note that our restriction to local exposure means that nonlocal impacts of extreme events are not included in our estimates. Examples for such nonlocal impacts include the impact of crop failure on food security through trade (d'Amour et al., 2016; Puma et al., 2015), the amplifying effect of increased upstream water demand on downstream water scarcity during drought (Veldkamp et al., 2017), and the impact of wildfires on urban air quality (Konovalov et al., 2011).

We aggregate exposure across event categories to measure the overall exposure to extreme climate impact events. As for the individual categories, we measure the land area exposed to at least one event in a given

year, but this event may come from any of the categories we wish to aggregate. Since we do not know how land-area fractions exposed to different categories of events overlap at the subgrid scale, we assume that the land area fractions exposed overlap as much as possible except for the land area fractions exposed to crop failure and wildfire, which we assume to overlap as little as possible because crop land is explicitly unable to burn in all but one GVM (see Text S3). In line with these assumptions, we estimate the aggregated land area exposed as the maximum (sum in the case of crop failure and wildfire) of the land area fractions exposed to events from the individual categories to be aggregated. Population exposure is aggregated similarly but using the maximum in all cases because the population fractions exposed to crop failure and wildfire are not necessarily disjoint. Note that our aggregation method prevents the double counting of related events such as co-occurring droughts and wildfires.

2.3. Pure Effect of Climate Change

Two types of impact model simulations are analyzed in this study. The first type are *scenario* simulations that use historical and projected climate input data before and after 2005, respectively, combined with input data on direct human influences that mimic the historical socioeconomic development until 2005 and are fixed at 2005 levels thereafter. Direct human influences considered in these simulations include but are not limited to land, water and fertilizer use. In some cases the historical scenario simulations were also done using fixed socioeconomic input data, sometimes due to a lack of historically varying data (such as for growing seasons and fertilizer input), and in other cases due to limited resources for input data preprocessing (such as for H08 and JULES-W1) or a model's inability to work with time-varying input data (such as transient land cover for WaterGAP2 and CLM4.5 with active irrigation). For an overview of which and how direct human influences are considered in the GHM, GGCM, and GVM simulations see Table S4.

The second type are *baseline* simulations that use the same input data on direct human influences as the scenario simulations but combine these with climate input data that represent counterfactually stable preindustrial conditions for the entire 1861–2100 time period. The *pure effect of climate change* on the land area and population exposed to extreme events is derived from differences between scenario and baseline simulations.

We pool these differences from the historical, RCP2.6, and RCP6.0 scenario simulations to quantify changes in exposure at different levels of global warming. This pooling is done under the assumption that the relationship between global mean temperature (GMT) change and exposure change is scenario-independent. For the pooling we use GMT change bins of 0.5°C width covering the -0.5°C to 4.0°C GMT change range (see Table S5 for the GCM-specific number of simulation years per bin). The pooled differences are then averaged per bin and mean values of these averages from neighboring bins are used to quantify the change in exposure at global warming levels that increase from 0°C to 3.5°C in steps of 0.5°C relative to the GCM-specific preindustrial average GMT level.

2.4. Extreme Event Definitions

Six categories of extreme events are analyzed in this study. We distinguish *extensive* events (droughts and heatwaves) to which any part of a grid cell is susceptible, from *confined* events (river floods, tropical cyclones, crop failure, and wildfires) to which only parts of a grid cell may be susceptible according to elevation maps, storm tracks, land use patterns, or vegetation structure. The distinction reflects that we expect absolute changes in exposure to be larger for extensive than for confined events. In line with this expectation, aggregated exposure is analyzed not only for all event categories combined but also for extensive events and confined events separately. In the following we present the details of our extreme event definitions. An overview is given in Table 1.

Since the GHMs do not directly simulate flooded area, we employ the flood inundation scheme of the global river model CaMa-Flood to translate daily runoff from the GHMs into flood depth and flooded area. Specifically, the flooded area associated with the annual maximum daily discharge is used to estimate the land area exposed to river flooding at least once in a given year. A grid cell is considered to be exposed to river flooding if the maximum annual discharge exceeds the 100-year return level derived from the preindustrial baseline simulations. To estimate the flooded area fraction of a $0.5° \times 0.5°$ grid cell, we downscale CaMa-Flood output of flood depth to 2.5′ spatial resolution using high-resolution topography data and aggregate the resulting flooded area back up to 0.5° resolution (see Text S1 for details).

Table 1
Extreme Event Definitions Used in This Study

Event category	Event type	Definition of land area exposed	Definition of population exposed
River flood	Confined (by topography)	Flooding is assumed to occur whenever daily discharge (0.5° resolution) exceeds the preindustrial 100-year return level; to derive the associated land area exposed per grid cell, simulated runoff is translated into inundation areas (2.5′ resolution) by CaMaFlood (Yamazaki et al., 2011, 2013).	Land area fraction exposed multiplied by total population of grid cell.
Tropical cyclone	Confined (to storm track)	Fraction of grid cell exposed to 1-min sustained hurricane-force winds (at least 64 kt) at least once a year (0.1° resolution); information required about wind fields is derived from center location and minimum pressure/maximum wind speed (Emanuel, 2013; Geiger et al., 2018).	Land area fraction exposed multiplied by total population of grid cell.
Crop failure	Confined (to agricultural land)	Fraction of grid cell where one of the considered crops (maize, wheat, soybean, and rice) is grown and the corresponding crop yield falls short of the 2.5th percentile of the preindustrial baseline distribution; crop-specific land area fractions exposed are added up.	Land area fraction exposed multiplied by employment in agriculture as a fraction of total employment, divided by grid cell area fraction used for agriculture.
Wildfire	Confined (to vegetated land)	Annual aggregate of monthly burned land area simulated by global vegetation models.	Burned land area fraction multiplied by total population of grid cell.
Drought	Extensive (can occur everywhere)	Entire grid cell if monthly soil moisture falls below the 2.5th percentile of the preindustrial baseline distribution for at least seven consecutive months.	Rural population (Klein Goldewijk et al., 2017) of exposed grid cell.
Heatwave	Extensive (can occur everywhere)	Entire grid cell if both, a relative indicator based on temperature (Russo et al., 2015, 2017) and an absolute indicator based on temperature and relative humidity (Masterton & Richardson, 1979) exceed their respective threshold value.	Total population of exposed grid cell.

The land area exposed to tropical cyclones is defined as the land area that is subject to 1-min sustained hurricane-force winds (wind speed of at least 64 knots) at least once in a given year. For each year and each realization of cyclone tracks a binary map of exposed land area is generated at 0.1° spatial resolution. This map is then aggregated to obtain the land area fraction exposed at 0.5° spatial resolution. Details of the generation of cyclone track realizations are given in Text S5. Note that our definition of exposure to tropical cyclones omits the exposure to storm surge and heavy precipitation that generally occur in association with a tropical cyclone. Since these byproducts may strike beyond the region exposed to hurricane-force winds we consider our tropical cyclone exposure to be conservative.

Crop failure is separately defined for each grid cell and crop type (maize, rice, soybean, and wheat) distinguishing between irrigated and rainfed yields. A crop is defined to fail if its yield falls below the 2.5th percentile of the baseline yield distribution derived from the associated preindustrial baseline simulation. The land area fraction exposed to crop failure is set equal to the land area fraction used to grow the failed crop(s) in a given year and grid cell. Note that we consider crop failure as an individual event category, not as the potential result of a drought or heatwave. We do this because not every crop failure is caused by a

drought or heatwave (Kamali et al., 2018; Webber et al., 2020) and since crop failure is an important extreme climate impact event. For example, it may disrupt food security (Battisti & Naylor, 2009; Gaupp et al., 2019), which belongs to the 17 Sustainable Development Goals of the United Nations.

Exposure to wildfire is directly derived from monthly or annual output of burned area provided by the five GVMs. For the models that provide monthly burned area (VISIT, ORCHIDEE, and CARAIB), the annual land area fraction exposed to wildfire is calculated as the sum of the monthly values (capped at 100%). We thereby assume that an area that has burned during one month of a year is unlikely to burn again during the same year, because fires reduce the available fuel for the next burning and in most GVMs fire ignitions are limited by fuel availability. This mechanism holds true for most of the globe (Andela et al., 2017; Archibald et al., 2013; van der Werf et al., 2017), although fire return intervals may be smaller than one year in strongly fire-dominated ecosystems such as in Sub-Saharan Africa (Archibald et al., 2010).

We define a drought to occur if monthly mean root-zone soil moisture (see Text S2 for details) falls below the 2.5th percentile of the preindustrial baseline distribution for at least 7 consecutive months. While this time scale is in line with medium-term drought definitions used in other studies (Seneviratne et al., 2010; Sheffield & Wood, 2008), using soil moisture to identify drought conditions is less common. The most prominent drought indices, the Standard Precipitation Index and the Palmer Drought Severity Index, are defined based on meteorological variables (precipitation and temperature) (Heim, 2002; Seneviratne et al., 2010). Root-zone soil moisture has several advantages since it shows the combined effects of processes such as precipitation, soil evaporation, plant transpiration, infiltration, runoff, snow accumulation, and melt and is therefore a good indicator for drought conditions that are relevant in particular for plant growth and ecosystem respiration (Dai, 2013; Sheffield & Wood, 2008; Stocker et al., 2019). While using relative monthly thresholds to distinguish dry from wet periods is common (Hirabayashi et al., 2008; Nyabeze, 2004; Stahl, 2001; Vidal et al., 2010; Van Loon, 2015) and consistent with the other extreme event definitions it also means that our drought definition does not reflect absolute water availability. Therefore, exposure to drought as defined here should not be confused with exposure to water scarcity (water demand versus water supply), which is captured by socioeconomic drought indices (Mehran et al., 2015; Veldkamp et al., 2017).

Exposure to heatwaves is calculated directly from bias-adjusted GCM output of near-surface air temperature and relative humidity. Given the wide range of heatwave impacts and their various drivers, such as intensity and duration, the definition of a heatwave varies between studies according to the specific application (Perkins, 2015). Our heatwave definition combines a relative indicator, which assesses the magnitude of a heatwave relative to magnitudes that were normal under preindustrial climate conditions, with an absolute criterion that ensures that the heatwaves identified would not only be considered exceptionally warm under preindustrial climate conditions, but would also adversely affect human health. The relative indicator is based on the Heat Wave Magnitude Index daily (HWMId), which depends only on daily maximum temperature (Russo et al., 2015, 2017). The absolute indicator is the Humidex (Masterton & Richardson, 1979), which depends on daily maximum temperature as well as daily mean temperature and relative humidity. Including the Humidex, we make sure that our heatwaves are both hot and humid, and hence represent different conditions than our droughts. For details of our heatwave definition see Text S6.

As can be seen from our definitions, grid cells can be partially exposed to river floods, tropical cyclones, crop failure, and wildfires. This reflects that the spatial extent of those events is limited by topography, storm tracks, land use, and vegetation patterns, respectively. In contrast, grid cells can only be entirely exposed to droughts and heatwaves because their occurrence is computed from GHM and GCM output at 0.5° spatial resolution and downscaling those occurrences is less straightforward than for the confined events. While, for example, river floods have clear physical limits determined by topography, the spatial extent of droughts and heatwaves is less delineated by, for example, elevation, land cover, or soil type. Higher-resolution estimates of exposure to droughts and heatwaves would hence require higher-resolution climate input data.

3. Results

3.1. Global Scale

The pure effect of climate change on the global exposure of land and population to extreme events is depicted in Figures 1 and 2, respectively. Shown are absolute changes in exposure according to individual climate model-impact model combinations (for the corresponding relative changes see Figures S1–S9) as well as

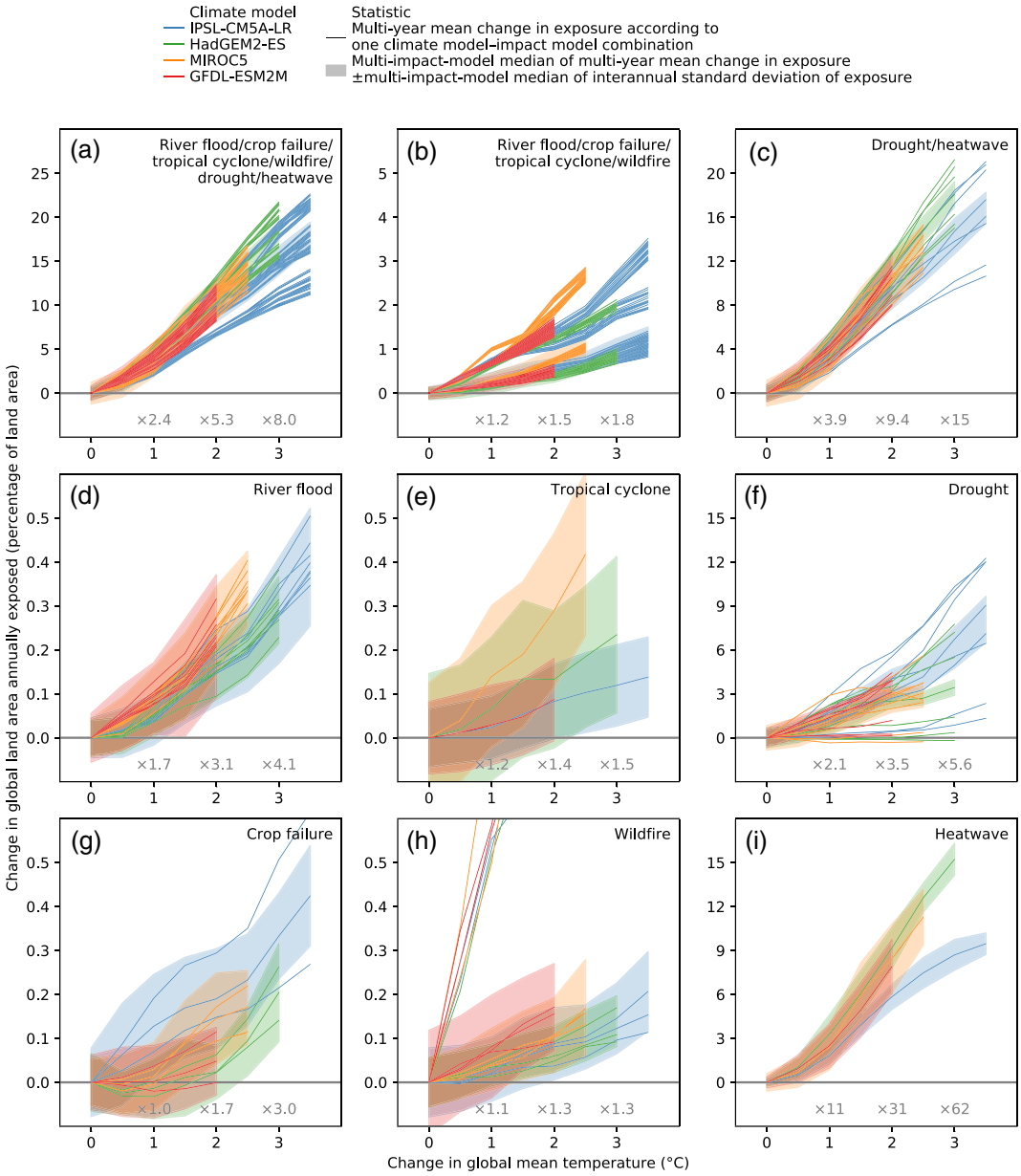

Figure 1. Change in global land area annually exposed to extreme events at different levels of global warming relative to preindustrial climate conditions. Changes are expressed as percentages of the total global land area excluding Greenland and Antarctica. Every line represents the warming level-dependent multiyear mean change in exposure according to one climate model-impact model combination. Different colors indicate results for different climate models. Shaded areas represent the multi-impact-model median of the multiyear mean change in exposure ± the multi-impact-model median of the interannual standard deviation of exposure. Gray numbers at the bottom of each panel indicate multimodel median change factors at 1°C, 2°C, and 3°C global warming relative to preindustrial conditions. Panels (a)–(c) and (d)–(i) show results for aggregated and individual event categories, respectively. See Figures S1–S6 for which impact model is behind which line in panels (d)–(i).

multimodel median change factors, where a change factor of 3 indicates an increase by a factor of 3, which is equivalent to a relative increase of 200%.

According to our simulations, the historical global warming of 1°C has already substantially increased the global land area annually exposed to extreme events. Compared to a counterfactual world with preindustrial climate conditions and today's socioeconomic background conditions, today's exposure is already 2.4 times larger (Figure 1a; central 90% multimodel range: 1.5–3.2). All categories of extreme events have contributed

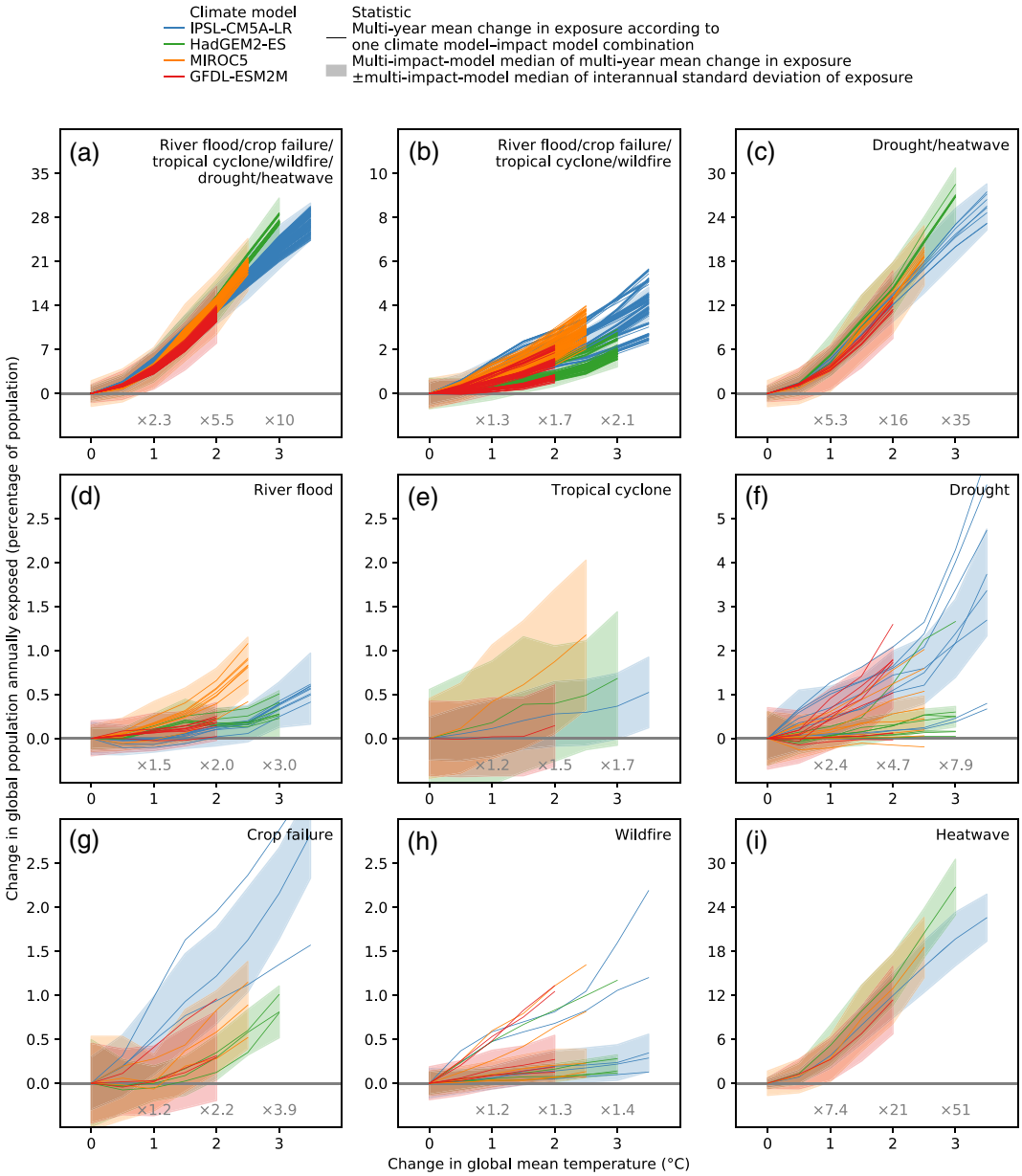

Figure 2. Change in global population annually exposed to extreme events at different levels of global warming relative to preindustrial climate conditions. Analogous to Figure 1, with changes expressed as percentages of the global population of year 2005.

to this increase, but changes in droughts and heatwaves dominate the overall signal (Figures 1b–1i). For ongoing global warming of up to 3.5°C relative to preindustrial conditions, we project the global land area exposed to extremes to increase further for all event categories. In particular, global warming by 2°C and 3°C is projected to increase the land area annually exposed to extreme events by a factor of 5.3 and 8.0, respectively (Figure 1a; central 90% multimodel range: 2.6–7.3 and 3.5–11, respectively). Results for 3°C global warming are more uncertain since only two out of four GCMs reach this warming level under RCP6.0.

In line with an increasing global land exposure, global warming is projected to increase the global population exposed to extreme events from each of the six categories considered here (Figure 2). For all six categories combined, we find that the historical 1°C global warming has already increased global exposure by a factor of 2.3 (Figure 2a; central 90% multimodel range: 1.8–3.6). Compared to increases in the global land area fraction exposed, increases in the global population fraction exposed are greater for tropical cyclones, crop failure and heatwaves, approximately equal for river floods and wildfires, and less for droughts. These differences

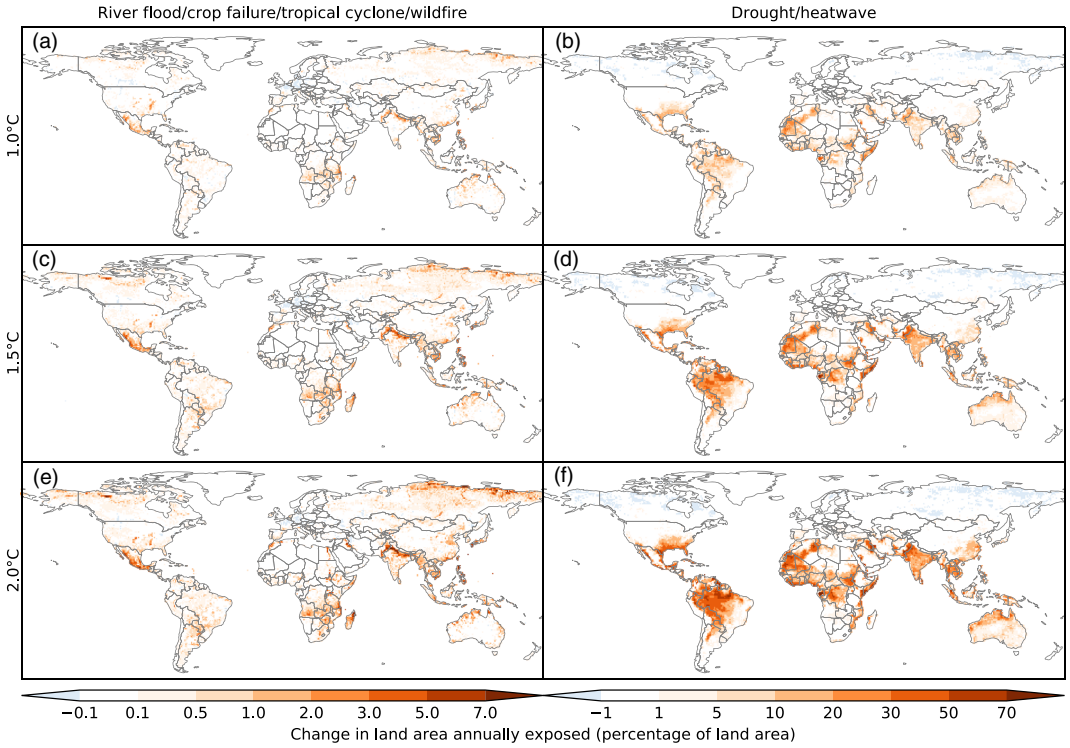

Figure 3. Change in land area annually exposed to extreme events at the grid scale for different levels of global warming relative to preindustrial climate conditions. Changes are expressed as percentages of the land area of each 0.5° × 0.5° grid cell. Colors indicate multimodel median changes in multiyear mean land area exposed to (a, c, and e) confined events and (b, d, and f) extensive events at (a, b) 1°C, (c, d) 1.5°C, and (e, f) 2°C global warming. White indicates missing data over Greenland and a small change or less than 66% model agreement on the sign of the change elsewhere.

reflect that tropical cyclones primarily hit the densely populated coastal regions of the tropics and subtropics, crops are usually grown in close proximity to human settlements, and (humid) heatwaves primarily strike the densely populated low-latitude and low-altitude regions of the world, whereas the regions most prone to droughts are typically sparsely populated.

Projected changes come with varying degrees of modeling uncertainty. While for heatwaves, the climate change signal is particularly large relative to interannual variability, and differences between climate models are particularly small in comparison, the opposite is true for tropical cyclones. Nevertheless, for both event categories, all four climate models project an increase in exposure. For the other four event categories, the relative share of the overall modeling uncertainty of climate models and impact models varies. For river floods and crop failure, the climate models contribute the bulk of the modeling uncertainty. In contrast, for droughts and wildfires, modeling uncertainty is dominated by the impact models.

Changes in global land area and population exposure are about one order of magnitude larger for extensive compared to confined events. This is also true for the corresponding relative changes (expressed as multimodel median change factors in Figures 1 and 2 and shown for individual models and event categories in Figures S1–S6). Note that for tropical cyclones, droughts, and wildfires, the modeling uncertainty of relative changes in global exposure is lower than the modeling uncertainty of changes in global exposure. The opposite is true for heatwaves and there is no difference for river floods and crop failure.

3.2. Grid Scale

We now turn to the grid scale to identify the regions most exposed to extreme climate impact events in the future. Projections indicate that most regions of the world will face increases in land exposure to extremes (Figure 3, see Figures S10–S15 for individual category results). Particularly large increases in the land area annually exposed to confined events are projected for the Midwestern United States (mainly driven by

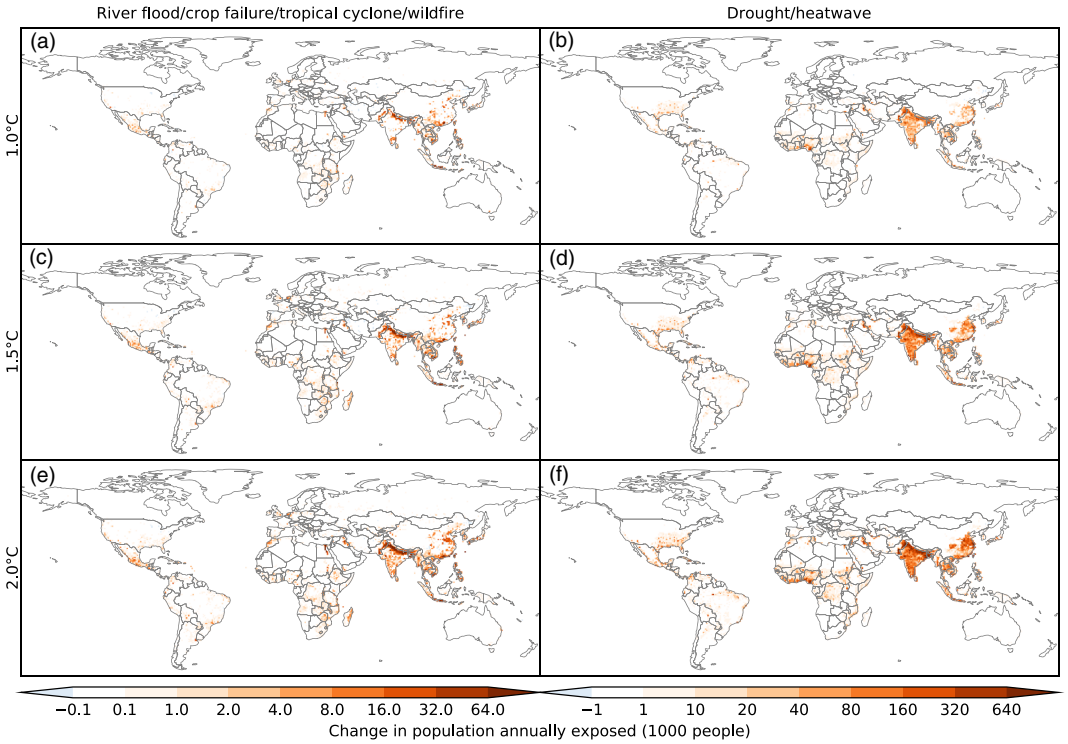

Figure 4. Change in population annually exposed to extreme events at the grid scale for different levels of global warming relative to preindustrial climate conditions. Analogous to Figure 3, with changes expressed in thousands of people based on the population distribution of year 2005.

crop failure), Mexico (mainly driven by tropical cyclones, crop failure, and wildfires), South America and Southern Africa (mainly driven by wildfires), the Nile valley and East Africa (mainly driven by river floods and tropical cyclones), North Africa, the Middle East, and South Asia (mainly driven by crop failure), Southeast Asia (mainly driven by tropical cyclones and river floods), East China (mainly driven by tropical cyclones and crop failure), Japan (mainly driven by tropical cyclones), Northern Canada and Russia (mainly driven by river floods), and Australia (mainly driven by tropical cyclones and wildfires).

Large increases in the land area annually exposed to extensive events are projected for many tropical and subtropical regions. While most of these increases are driven by heatwaves, increases in land area exposed to drought are projected for large parts of South America, Southern Europe, the Middle East, and North Africa, as well as for small parts of Sub-Saharan Africa, China, and Australia. Decreases in exposure to drought are projected for Northern Canada and Russia.

The corresponding changes in population exposure are greatest where increases in land exposure meet high population density (Figure 4). These regions are West Africa, South Asia, East Asia, and Southeast Asia. The largest increases in population exposure to confined and extensive events are concentrated in South Asia, in particular in the Indo-Gangetic Plain.

3.3. National Scale

National-scale projections of land and population exposure to extreme climate impact events of any category are shown in Figures 5 and 6. In line with grid-scale results, particularly large increases in population exposure are projected for the South Asian countries Pakistan, India, and Bangladesh, mainly driven by increases in exposure to heatwaves and crop failure. In agreement with results at the global scale, modeling uncertainty is particularly large for wildfires and droughts. It is smaller for river floods, tropical cyclones, and crop failure. The clearest climate change signal is simulated for heatwaves.

The largest increases in population exposure to river floods are projected for Egypt, Sudan, and the Netherlands. For tropical cyclones, the largest increases are projected for the Comoros, the Philippines, and Solomon Islands. For crop failure, the largest increases are projected for Iraq, Egypt, and Nepal. For wildfires,

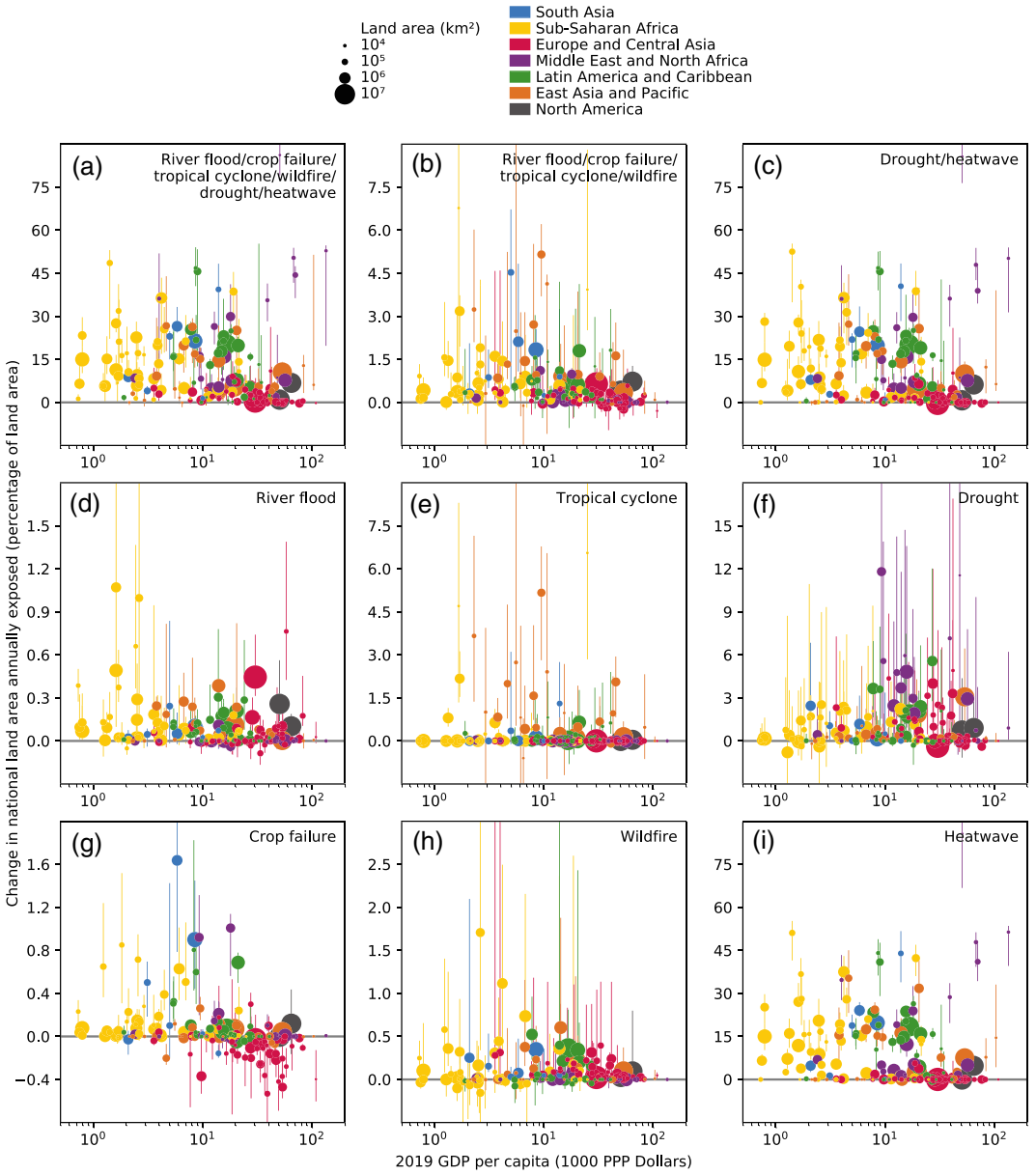

Figure 5. Change in national land area annually exposed to extreme events for 2°C global warming relative to preindustrial climate conditions. Changes are expressed as percentages of the national land area and plotted against 2019 GDP per capita (IMF, 2019). Every circle represents the multimodel median change in the multiyear mean land area exposed for one country. The vertical line behind a circle represents the corresponding multimodel interquartile range. Circle color and circle area represent world region and national land area, respectively. Panels (a)–(c) and (d)–(i) show results for aggregated and individual event categories, respectively.

increases are largest for Zimbabwe, Angola, and Mongolia. For droughts, the largest increases are projected for Morocco, Israel, and Algeria. For heatwaves, the largest increases are projected for Bahrain, Kuwait, and Guyana.

To highlight distributional aspects of climate change, Figures 5 and 6 relate projected changes in exposure to 2019 gross domestic product (GDP) per capita at purchasing power parity (PPP). We find that changes in exposure to river floods, tropical cyclones, wildfires, and droughts are only weakly related to GDP. In contrast, changes in exposure to crop failure and heatwaves are unevenly distributed.

Exposure to crop failure is projected to increase for most low-income and middle-income countries whereas it is projected to decrease for most high-income countries. In particular, decreases are projected for most

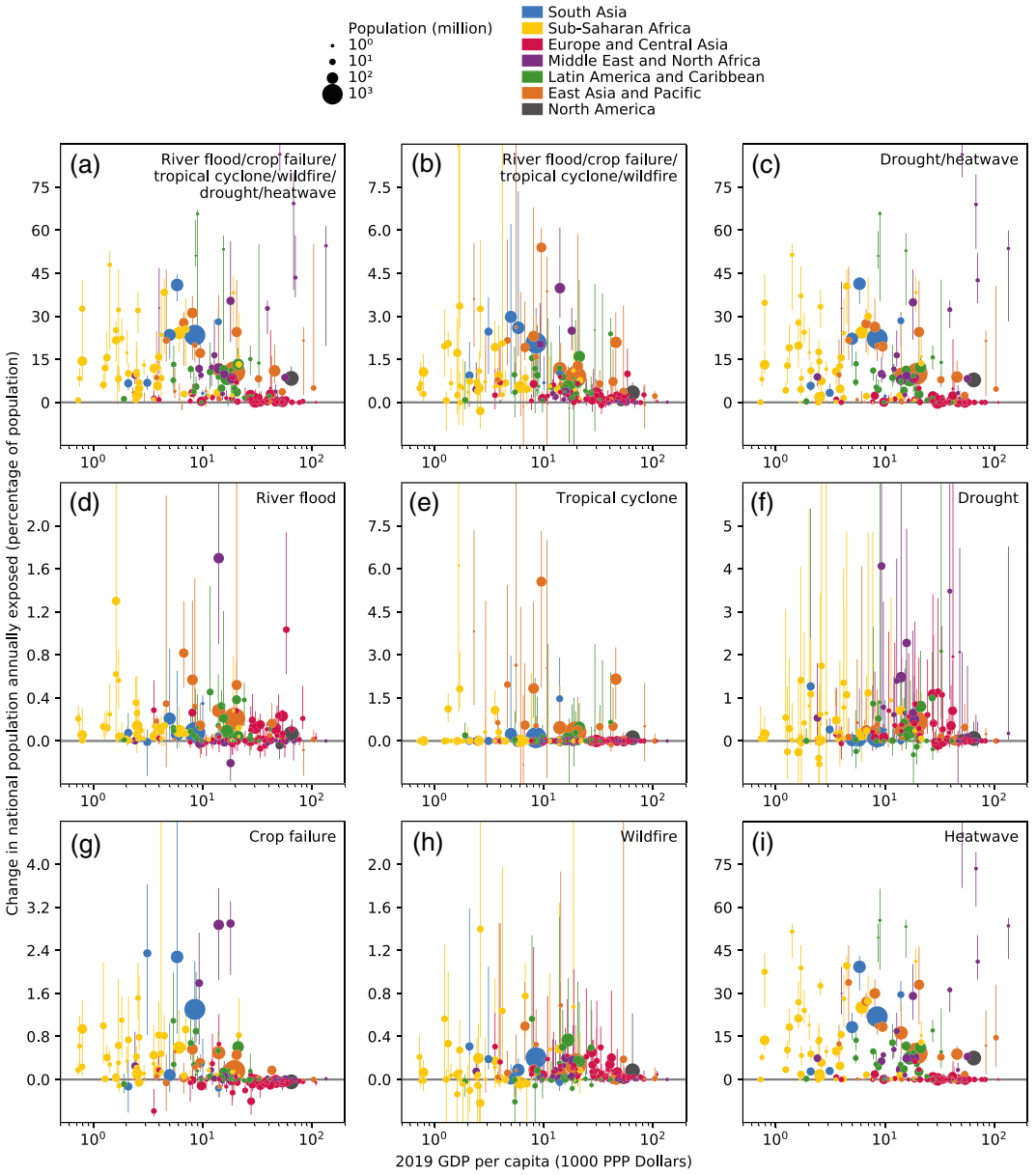

Figure 6. Change in national population annually exposed to extreme events for 2°C global warming relative to preindustrial climate conditions. Analogous to Figure 5, with changes expressed as percentages of the national population of year 2005.

countries in Europe and Central Asia. In many of those cases, decreases in land exposure are greater than decreases in population exposure since the latter are limited by low population fractions working in agriculture.

Particularly large increases in exposure to heatwaves are projected for the countries around the Persian Gulf. Apart from that region, exposure to heatwaves is projected to increase more in low-income and middle-income countries than in high-income countries. For Canada and most countries in Europe and Central Asia, we project no change in exposure to heatwaves as long as global warming is limited to 2°C. This finding is related to our heatwave definition which requires heatwaves to be both hot and humid (Text S6). Below 2°C global warming, the Humidex hardly ever exceeds our threshold value of 45 in the temperate zones and polar regions.

4. Discussion

Our findings paint a clear picture of the impacts of global warming on extremes. In particular the increase in global exposure to extremes that we project for all six event categories is a strong result that needs to be discussed, since it is associated with uncertainties from many sources, including climate and impact modeling uncertainties, limitations of our exposure measures and extreme event definitions, and omitted effects of future population change, economic development, and adaptation. Fundamental limitations of the impact models, exposure measures, and extreme event definitions used here have already been presented in section 2. We now expand on that discussion and compare our findings to those of other studies. The numbers presented here for relative changes in exposure represent the multimodel median as well as the central 90% multimodel range (in parentheses).

Global warming of 2°C is projected to increase the global population exposure to river floods by 100% (60–310). River flood modeling uncertainty is mostly related to climate input data uncertainty. This finding is supported by previous studies (Giuntoli et al., 2015; Hattermann et al., 2018; Velázquez et al., 2013; Vetter et al., 2017), which found GCMs to contribute more to high-flow modeling uncertainty than GHMs. The high uncertainty in climate input data is in turn related to the poor reproduction of extreme precipitation events by GCMs, due to their coarse resolution and deficient parametrization of the complex multiscale processes involved in cloud dynamics (Lange et al., 2015; Randall et al., 2003). Consequently, precipitation projections are uncertain (Stocker et al., 2013) and it is expected that, using only four GCMs, we do not cover the full range of uncertainty of river flood projections. Nonetheless, our qualitative finding of an increase of the land area exposed to river floods in a warmer world is in line with more frequent extreme precipitation events that are expected from thermodynamic theory (Allen & Ingram, 2002), found in observations (Lehmann et al., 2015), and projected by climate models (Ban et al., 2015). The spatial pattern of change in exposure to formerly 100-year river floods found here does not fully agree with the projections by Hirabayashi et al. (2013). Given the high climate modeling uncertainty of river flood projections, we suspect that these deviations are due to different climate model outputs used here (precipitation, temperature, and radiation from four GCMs) and in their study (runoff from eleven GCMs). Another caveat is that while dams and levees are often effective measures to prevent river flooding, river flood defense in most developing regions are currently insufficient to prevent 100-year return level floods (Scussolini et al., 2016). Assuming universal protection against river floods with return periods shorter than 100 years is thus expected to underestimate flooded area in developing countries, but overestimate it in some industrialized countries (such as the Netherlands, see Figure 5). Since few regions currently have protection levels greater than 100-year return levels, higher exposure to flooding than projected here should be expected in most regions.

We project a 50% (10-110) increase of the global population annually exposed to tropical cyclones in response to 2°C global warming. Similarly large uncertainties were found in projections done with older versions of the same tropical cyclone model as used in this study (Emanuel, 2013; Emanuel et al., 2008). We simulate particularly large exposure increases for the island countries in the Indian and Pacific oceans. Those increases are related to either constant or increasing tropical cyclone frequencies and intensities that our tropical cyclone model projects for all ocean basins and climate input data sets. While an increase in tropical cyclone intensity with global warming is in line with maximum potential intensity theory and climate model projections done with coarse-resolution GCMs as well as convection-permitting regional climate models (Bender et al., 2010; Emanuel, 1987; Knutson & Tuleya, 2004; Patricola & Wehner, 2018; Sobel et al., 2016), an increase in tropical cyclone frequency with global warming is less supported by earlier findings since most (Emanuel et al., 2008; Gualdi et al., 2008; Knutson et al., 2010; Walsh et al., 2016; Wehner et al., 2018), but not all (Lee et al., 2020; Vecchi et al., 2019) models project fewer tropical cyclones in a warmer world. While this suggests that we overestimate the increase in global exposure to tropical cyclones, the increase we find may still hold, since Mendelsohn et al. (2012) and Gettelman et al. (2018) found that an increase in cyclone intensity has the potential to overcompensate for a decrease in the number of tropical cyclones, resulting in a net increase in global exposure to tropical cyclones in response to global warming. Note that future adaptation has the potential to reverse any such trend given the large potential impact of socioeconomic change on tropical cyclone exposure (Bouwer, 2013; Gettelman et al., 2018; Peduzzi et al., 2012; Pielke, 2007).

Global population exposure to crop failure is projected to increase by 120% (50–380) in response to 2°C global warming. We find that GCMs contribute more to the modeling uncertainty than GGCMs. In contrast, previous analyses of variance of crop yields projected in multimodel frameworks attributed larger variance

fractions to crop models than to climate models (Ostberg et al., 2018; Tao et al., 2018). Given that our GGCM ensemble only has three members, this suggests that we underestimate the structural uncertainty of our crop failure projections. However, the importance of differences in climate projections for simulated extreme yields has not been explored to date. Our finding that global warming increases the exposure of tropical and subtropical regions to crop failure in particular for maize and wheat is in line with earlier findings (Challinor et al., 2014; Knox et al., 2012; Rosenzweig et al., 2014). According to our multimodel median projections, increases in global exposure to crop failure only set in at about 1°C global warming relative to preindustrial conditions. This is explained by northern regions seeing a decrease in exposure at low warming levels that balances the concurrent increase at lower latitudes. Such initially opposing signals in different regions have also been found in studies of climate change impacts on multiyear mean yields (Franke et al., 2019; Minoli et al., 2019). The decrease in exposure to crop failure we find for the northern parts of Europe and Central Asia beyond 1°C global warming is in line with previous crop yield projections for these regions (Knox et al., 2016; Reyer et al., 2017). A major source of uncertainty in our crop yield projections is the CO_2 fertilization effect, since both the magnitude of the effect itself and the atmospheric CO_2 concentration at a given global warming level are subject to considerable uncertainty (Deryng et al., 2016; Rosenzweig et al., 2014; Schleussner et al., 2018). Note that our crop models do not account for changes in agricultural management, such as changes in the use of cultivars, fertilizer, pesticides, and irrigation. Therefore, positive effects of future adaptation are not included in our crop yield projections in spite of their potential to make up for at least some of the projected yield decreases (Challinor et al., 2014; Minoli et al., 2019).

Global warming of 2°C is projected to increase the global population exposure to wildfires by 30% (10–140). Modeling uncertainty is dominated by the GVMs, with ORCHIDEE and VISIT simulating substantially larger absolute increases in annual global burned area than the other three GVMs. Since this wide range of changes largely reflects differences in baseline values (Text S3), relative changes are more informative than absolute changes (Figure S4). The large structural wildfire modeling uncertainty found here resembles results of earlier model intercomparison studies (Andela et al., 2017; Forkel et al., 2019; Wu et al., 2015). Note that our GVMs have only a very limited and simplified representation of direct human influences on wildfire ignition, suppression and management. Therefore, the projected increase in annual global burned area should be interpreted as a purely climate-driven increase in wildfire risk with global warming. Such an increase is consistent with earlier findings (Abatzoglou et al., 2019; Jolly et al., 2015; Pechony & Shindell, 2010; Turco et al., 2018), but we acknowledge that future changes in direct human influences on wildfires have the potential to reverse this trend, as they have done in the past (Andela et al., 2017; Forkel et al., 2019; Yang et al., 2014).

We project a 370% (30–790) increase of the global population annually exposed to droughts in response to 2°C global warming. Drought modeling uncertainty is mainly driven by the GHMs. Larger contributions by GCMs to drought modeling uncertainty was found by Samaniego et al. (2017), where multimodel projections of hydrological droughts at the river basin scale were analyzed. In contrast, larger uncertainty due to GHMs than GCMs was found by Prudhomme et al. (2014) in multimodel grid-scale projections of hydrological droughts. While seven out of eight GHMs project global warming to increase the global land area annually exposed to droughts, H08 projects a decrease for two out of four GCMs (Figure S5). In these two cases, decreases in the boreal Northern Hemisphere overcompensate for increases in most other regions. The other seven models project larger increases in most regions and in some cases not even a decrease in the boreal Northern Hemisphere, despite the increase in precipitation projected there. It is possible that GHMs at the high end of our ensemble overestimate increases in exposure to drought since some of the models' potential evaporation schemes have been shown to produce dry biases in future projections (Milly & Dunne, 2017). Yet Dai (2013), Prudhomme et al. (2014), and Lehner et al. (2017) support our finding of an increasing global exposure to drought under global warming, and the spatial patterns of change largely agree, with particularly large increases in drought exposure projected for the Mediterranean region and the Amazon basin.

Global population exposure to heatwaves is projected to increase by 2,000% (1,500–3,400) in response to 2°C global warming. Modeling uncertainty originates from differences in regional patterns of temperature and relative humidity change projected by the GCMs. However, the uncertainty is limited by the thermodynamic relationship between those two variables (Fischer & Knutti, 2013). Since our heatwave definition takes humidity into account, our findings compare well with studies that define heatwaves based on wet-bulb

temperature (Dunne et al., 2013; Im et al., 2017; Sherwood & Huber, 2010). In particular, spatial patterns agree, with particularly large increases in exposure to heatwaves projected for the Persian Gulf and the Indo-Gangetic Plain. The rate of change in global exposure to heatwaves found here compares well with results in Dosio et al. (2018), even though they use a heatwave definition that does not take humidity into account. Dosio et al. (2018) find that, compared to a 1.5°C world, under 2°C global warming the frequency of extreme heatwaves would double over most of the globe. For the same change in global mean temperature, we project a 50% increase in the global land area (excluding Greenland and Antarctica) annually exposed to heatwaves. Note that our estimates do not account for future adaptation or population change. Both are considered to be sources of considerable uncertainty for projections of population exposure to heatwaves (Mendelsohn, 2006; Perkins, 2015). For example, we do not consider future urbanization, which has the potential to further increase population exposure to heatwaves due to the urban heat island effect (Fischer et al., 2012; Oleson et al., 2011).

Our finding that poorer countries will be disproportionally exposed to crop failure and heatwaves extends earlier analyses of distributional aspects of climate change that focused on exposure to temperature extremes (Harrington et al., 2016, 2018). Our result also corroborates and complements earlier findings that macroeconomic impacts of climate change are larger in low than high-latitude countries and that the poor may bear the brunt of the economic damages from climate change (Burke et al., 2015; Diffenbaugh & Burke, 2019; Hansen & Sato, 2016; King & Harrington, 2018; Mahlstein et al., 2011; Mendelsohn et al., 2006; Schelling, 1992; Tol, 2018). In this context it should be noted that the present analysis only considers exposure and is therefore not a complete climate change risk assessment because such an assessment would have to include vulnerability (Field et al., 2014). Since vulnerability to extreme climate impact events tends to be higher in poorer countries (Diffenbaugh et al., 2007), disparities in climate change risks between poor and rich countries are expected to be even larger than the disparities in exposure found here. That being said, they are also considerably more uncertain due to the strong dependence of risk on vulnerability and the uncertain future development of vulnerability (Byers et al., 2018; Schelling, 1992).

5. Conclusion

Using an innovative experimental setup, this study quantifies the pure effect of climate change on the land area and population exposed to six categories of extreme climate impact events (river floods, tropical cyclones, crop failure, wildfires, droughts, and heatwaves) at the global, grid, and national scale.

For all six event categories combined, we find that the historical 1°C global warming has already increased the global land area and population annually exposed by about 140% and 130%, respectively. While all six event categories contribute to these increases, droughts and heatwaves are the biggest contributors. These patterns are projected to intensify in response to ongoing global warming. For all six event categories combined and the 0–3°C warming level range, we simulate a continuous increase with global warming of both the annually exposed global land area and population. Results at the grid and national level indicate that most of the larger increases will occur in the tropical and subtropical regions, particularly in South Asia.

While our findings come with uncertainties from many sources, none of these uncertainties are likely to undermine our main conclusions: Anthropogenic climate change has already substantially increased the exposure to extreme climate impact events worldwide, and further global warming is projected to exacerbate the patterns of change we already see today. Our results support the claim that "holding the increase in the global average temperature to well below 2°C […] would significantly reduce the risks and impacts of climate change" (UNFCCC, 2016) and therefore underscore the urgency for climate action expressed in the Paris Agreement of 2015.

Data Availability Statement

The ISIMIP2b climate input data and impact model output data analyzed in this study are available in the ISIMIP data repository at ESGF, see https://esg.pik-potsdam.de/search/isimip/?project=ISIMIP2b&product=input and https://esg.pik-potsdam.de/search/isimip/?project=ISIMIP2b&product=output, respectively. More information about the GHM, GGCM, and GVM output data is provided by Gosling et al. (2020), Arneth et al. (2020), and Reyer et al. (2019), respectively. The tropical cyclone track data are available for research purposes from K. E. (emanuel@mit.edu) on request. Researchers will be asked to sign a nonredistribution agreement and to assert that the data will be used for nonprofit research only.

Acknowledgments
We thank the editor and two anonymous reviewers for constructive feedback. We thank three other anonymous reviewers for helpful comments on an earlier version of this paper submitted to a different journal. This research was supported in part by the German Federal Ministry of Education and Research (BMBF, grant numbers 01LS1201A2, 01LS1711F, and 01LA1829A) and the EU FP7 HELIX project (grant number 603864). Some authors acknowledge support from the Leibniz Competition projects SAW-2013-PIK-5 (EXPACT) and SAW-2016-PIK-1 (ENGAGE). Some authors acknowledge funding from the European Union's Horizon 2020 research and innovation program under grant agreement number 821010 (CASCADES). N. H., K. N., and Y. H. acknowledge support from the ERTD Funds 2RF-1802 and S-14 of the Environmental Restoration and Conservation Agency of Japan. W. T. was supported by an ETH Zurich postdoctoral fellowship (Fel-45 15-1). V. H. was supported by the Spanish Ministry of Economy, Industry and Competitiveness (MINECO, grant number PCIN-2017-046). P. C. acknowledges support from the CLAND ANR Convergence Institute. S. L. acknowledges funding from the European Union's Horizon 2020 research and innovation program under grant agreement number 641816 (CRESCENDO). Open access funding enabled and organized by Projekt DEAL.

References

Abatzoglou, J. T., & Williams, A. P. (2016). Impact of anthropogenic climate change on wildfire across western US forests. *Proceedings of the National Academy of Sciences*, *113*(42), 11,770–11,775. https://doi.org/10.1073/pnas.1607171113

Abatzoglou, J. T., Williams, A. P., & Barbero, R. (2019). Global emergence of anthropogenic climate change in fire weather indices. *Geophysical Research Letters*, *46*, 326–336. https://doi.org/10.1029/2018GL080959

Allen, M. R., & Ingram, W. J. (2002). Constraints on future changes in climate and the hydrologic cycle. *Nature*, *419*(6903), 228–232. https://doi.org/10.1038/nature01092

Andela, N., Morton, D. C., Giglio, L., Chen, Y., van der Werf, G. R., Kasibhatla, P. S., et al. (2017). A human-driven decline in global burned area. *Science*, *356*(6345), 1356–1362. https://doi.org/10.1126/science.aal4108

Archibald, S., Lehmann, C. E. R., Gómez-Dans, J. L., & Bradstock, R. A. (2013). Defining pyromes and global syndromes of fire regimes. *Proceedings of the National Academy of Sciences*, *110*(16), 6442–6447. https://doi.org/10.1073/pnas.1211466110

Archibald, S., Scholes, R. J., Roy, D. P., Roberts, G., & Boschetti, L. (2010). Southern African fire regimes as revealed by remote sensing. *International Journal of Wildland Fire*, *19*(7), 861–878. https://doi.org/10.1071/WF10008

Arneth, A., Jägermeyr, J., Rabin, S., Folberth, C., Khabarov, N., Liu, W., et al. (2020). ISIMIP2b simulation data from agricultural sector. https://doi.org/10.5880/PIK.2020.003

Aznar-Siguan, G., & Bresch, D. N. (2019). Climada v1: A global weather and climate risk assessment platform. *Geoscientific Model Development*, *12*(7), 3085–3097. https://doi.org/10.5194/gmd-12-3085-2019

Ban, N., Schmidli, J., & Schär, C. (2015). Heavy precipitation in a changing climate: Does short-term summer precipitation increase faster? *Geophysical Research Letters*, *42*, 1165–1172. https://doi.org/10.1002/2014GL062588

Battisti, D. S., & Naylor, R. L. (2009). Historical warnings of future food insecurity with unprecedented seasonal heat. *Science*, *323*(5911), 240–244. https://doi.org/10.1126/science.1164363

Bender, M. A., Knutson, T. R., Tuleya, R. E., Sirutis, J. J., Vecchi, G. A., Garner, S. T., & Held, I. M. (2010). Modeled impact of anthropogenic warming on the frequency of intense Atlantic hurricanes. *Science*, *327*(5964), 454–458. https://doi.org/10.1126/science.1180568

Bouwer, L. M. (2013). Projections of future extreme weather losses under changes in climate and exposure. *Risk Analysis*, *33*(5), 915–930. https://doi.org/10.1111/j.1539-6924.2012.01880.x

Burke, M., Hsiang, S. M., & Miguel, E. (2015). Global non-linear effect of temperature on economic production. *Nature*, *527*(7577), 235–239. https://doi.org/10.1038/nature15725

Byers, E., Gidden, M., Leclère, D., Balkovic, J., Burek, P., Ebi, K., et al. (2018). Global exposure and vulnerability to multi-sector development and climate change hotspots. *Environmental Research Letters*, *13*(5), 055012. https://doi.org/10.1088/1748-9326/aabf45

Challinor, A. J., Watson, J., Lobell, D. B., Howden, S. M., Smith, D. R., & Chhetri, N. (2014). A meta-analysis of crop yield under climate change and adaptation. *Nature Climate Change*, *4*, 287–291. https://doi.org/10.1038/nclimate2153

Coumou, D., & Rahmstorf, S. (2012). A decade of weather extremes. *Nature Climate Change*, *2*(7), 491–496. https://doi.org/10.1038/nclimate1452

d'Amour, C. B., Wenz, L., Kalkuhl, M., Steckel, J. C., & Creutzig, F. (2016). Teleconnected food supply shocks. *Environmental Research Letters*, *11*(3), 035007. https://doi.org/10.1088/1748-9326/11/3/035007

Dai, A. (2013). Increasing drought under global warming in observations and models. *Nature Climate Change*, *3*, 52–58. https://doi.org/10.1038/nclimate1633

Deryng, D., Elliott, J., Folberth, C., Müller, C., Pugh, T. A. M., Boote, K. J., et al. (2016). Regional disparities in the beneficial effects of rising co2 concentrations on crop water productivity. *Nature Climate Change*, *6*, 786. https://doi.org/10.1038/nclimate2995

Diffenbaugh, N. S., & Burke, M. (2019). Global warming has increased global economic inequality. *Proceedings of the National Academy of Sciences*, *116*, 9808–9813. https://doi.org/10.1073/pnas.1816020116

Diffenbaugh, N. S., Giorgi, F., Raymond, L., & Bi, X. (2007). Indicators of 21st century socioclimatic exposure. *Proceedings of the National Academy of Sciences*, *104*(51), 20,195–20,198. https://doi.org/10.1073/pnas.0706680105

Dosio, A., Mentaschi, L., Fischer, E. M., & Wyser, K. (2018). Extreme heat waves under 1.5°c and 2°c global warming. *Environmental Research Letters*, *13*(5), 054006. https://doi.org/10.1088/1748-9326/aab827

Dottori, F., Szewczyk, W., Ciscar, J.-C., Zhao, F., Alfieri, L., Hirabayashi, Y., et al. (2018). Increased human and economic losses from river flooding with anthropogenic warming. *Nature Climate Change*, *8*(9), 781–786. https://doi.org/10.1038/s41558-018-0257-z

Dunne, J. P., Stouffer, R. J., & John, J. G. (2013). Reductions in labour capacity from heat stress under climate warming. *Nature Climate Change*, *3*, 563. https://doi.org/10.1038/nclimate1827

Emanuel, K. (1987). The dependence of hurricane intensity on climate. *Nature*, *326*(6112), 483–485. https://doi.org/10.1038/326483a0

Emanuel, K. (2013). Downscaling CMIP5 climate models shows increased tropical cyclone activity over the 21st century. *Proceedings of the National Academy of Sciences*, *110*(30), 12,219–12,224. https://doi.org/10.1073/pnas.1301293110

Emanuel, K., Sundararajan, R., & Williams, J. (2008). Hurricanes and global warming: Results from downscaling IPCC AR4 simulations. *Bulletin of the American Meteorological Society*, *89*(3), 347–368. https://doi.org/10.1175/BAMS-89-3-347

Field, C. B., Barros, V. R., Dokken, D. J., Mach, K. J., Mastrandrea, M. D., Bilir, T. E., et al. (2014). *Climate change 2014: Impacts, adaptation, and vulnerability. Contribution of Working Group II to the fifth assessment report of the Intergovernmental Panel on Climate Change* (pp. 1–32). Cambridge, UK and New York, NY, USA: Cambridge University Press.

Fischer, E. M., & Knutti, R. (2013). Robust projections of combined humidity and temperature extremes. *Nature Climate Change*, *3*(2), 126–130. https://doi.org/10.1038/nclimate1682

Fischer, E. M., Oleson, K. W., & Lawrence, D. M. (2012). Contrasting urban and rural heat stress responses to climate change. *Geophysical Research Letters*, *39*, L03705. https://doi.org/10.1029/2011GL050576

Forkel, M., Andela, N., Harrison, S. P., Lasslop, G., van Marle, M., Chuvieco, E., et al. (2019). Emergent relationships with respect to burned area in global satellite observations and fire-enabled vegetation models. *Biogeosciences*, *16*(1), 57–76. https://doi.org/10.5194/bg-16-57-2019

Forkel, M., Dorigo, W., Lasslop, G., Chuvieco, E., Hantson, S., Heil, A., et al. (2019). Recent global and regional trends in burned area and their compensating environmental controls. *Environmental Research Communications*, *1*(5), 051005. https://doi.org/10.1088/2515-7620/ab25d2

Franke, J., Müller, C., Elliott, J., Ruane, A. C., Jagermeyr, J., Balkovic, J., et al. (2019). The GGCMI Phase II experiment: Global gridded crop model simulations under uniform changes in CO_2, temperature, water, and nitrogen levels (protocol version 1.0). *Geoscientific Model Development Discussions*, *2019*, 1–30. https://doi.org/10.5194/gmd-2019-237

Frieler, K., Lange, S., Piontek, F., Reyer, C. P. O., Schewe, J., Warszawski, L., et al. (2017). Assessing the impacts of 1.5 °C global warming—Simulation protocol of the Inter-Sectoral Impact Model Intercomparison Project (ISIMIP2b). *Geoscientific Model Development*, *10*(12), 4321–4345. https://doi.org/10.5194/gmd-10-4321-2017

Gaupp, F., Hall, J., Mitchell, D., & Dadson, S. (2019). Increasing risks of multiple breadbasket failure under 1.5 and 2°C global warming. *Agricultural Systems*, *175*, 34–45. https://doi.org/10.1016/j.agsy.2019.05.010

Geiger, T., Frieler, K., & Bresch, D. N. (2018). A global historical data set of tropical cyclone exposure (TCE-DAT). *Earth System Science Data*, *10*(1), 185–194. https://doi.org/10.5194/essd-10-185-2018

Geiger, T., Frieler, K., & Levermann, A. (2016). High-income does not protect against hurricane losses. *Environmental Research Letters*, *11*(8), 084012. https://doi.org/10.1088/1748-9326/11/8/084012

Geiger, T., & Stomper, A. (2020). Rising economic damages of natural disasters: Trends in event intensity or capital intensity? *Proceedings of the National Academy of Sciences*, *117*(12), 6312–6313. https://doi.org/10.1073/pnas.1922152117

Gettelman, A., Bresch, D. N., Chen, C. C., Truesdale, J. E., & Bacmeister, J. T. (2018). Projections of future tropical cyclone damage with a high-resolution global climate model. *Climatic Change*, *146*(3), 575–585.

Giuntoli, I., Vidal, J.-P., Prudhomme, C., & Hannah, D. M. (2015). Future hydrological extremes: The uncertainty from multiple global climate and global hydrological models. *Earth System Dynamics*, *6*(1), 267–285. https://doi.org/10.5194/esd-6-267-2015

Gosling, S. N., Müller Schmied, H., Burek, P., Chang, J., Ciais, P., Döll, P., et al. (2020). ISIMIP2b simulation data from water (global) sector. GFZ Data Services, https://doi.org/10.5880/PIK.2020.004

Gualdi, S., Scoccimarro, E., & Navarra, A. (2008). Changes in tropical cyclone activity due to global warming: Results from a high-resolution coupled general circulation model. *Journal of Climate*, *21*(20), 5204–5228. https://doi.org/10.1175/2008JCLI1921.1

Gudmundsson, L., Tallaksen, L. M., Stahl, K., Clark, D. B., Dumont, E., Hagemann, S., et al. (2012). Comparing large-scale hydrological model simulations to observed runoff percentiles in Europe. *Journal of Hydrometeorology*, *13*(2), 604–620. https://doi.org/10.1175/JHM-D-11-083.1

Hallegatte, S., Bangalore, M., Bonzanigo, L., Fay, M., Kane, T., Narloch, U., et al. (2015). *Shock waves: Managing the impacts of climate Change on poverty*. The World Bank. https://doi.org/10.1596/978-1-4648-0673-5

Hansen, J., & Sato, M. (2016). Regional climate change and national responsibilities. *Environmental Research Letters*, *11*(3), 034009. https://doi.org/10.1088/1748-9326/11/3/034009

Harrington, L. J., Frame, D. J., Fischer, E. M., Hawkins, E., Joshi, M., & Jones, C. D. (2016). Poorest countries experience earlier anthropogenic emergence of daily temperature extremes. *Environmental Research Letters*, *11*(5), 055007. https://doi.org/10.1088/1748-9326/11/5/055007

Harrington, L. J., Frame, D., King, A. D., & Otto, F. E. L. (2018). How uneven are changes to impact-relevant climate hazards in a 1.5°C world and beyond? *Geophysical Research Letters*, *45*, 6672–6680. https://doi.org/10.1029/2018GL078888

Hattermann, F. F., Vetter, T., Breuer, L., Su, B., Daggupati, P., Donnelly, C., et al. (2018). Sources of uncertainty in hydrological climate impact assessment: A cross-scale study. *Environmental Research Letters*, *13*(1), 015006. https://doi.org/10.1088/1748-9326/aa9938

Heim, R. R. (2002). A review of twentieth-century drought indices used in the United States. *Bulletin of the American Meteorological Society*, *83*(8), 1149–1166. https://doi.org/10.1175/1520-0477-83.8.1149

Hirabayashi, Y., Kanae, S., Emori, S., Oki, T., & Kimoto, M. (2008). Global projections of changing risks of floods and droughts in a changing climate. *Hydrological Sciences Journal*, *53*(4), 754–772. https://doi.org/10.1623/hysj.53.4.754

Hirabayashi, Y., Mahendran, R., Koirala, S., Konoshima, L., Yamazaki, D., Watanabe, S., et al. (2013). Global flood risk under climate change. *Nature Climate Change*, *3*(9), 816–821. https://doi.org/10.1038/nclimate1911

Hoegh-Guldberg, O., Jacob, D., Taylor, M., Bindi, M., Brown, S., Camilloni, I., et al. (2018). Impacts of 1.5°C global warming on natural and human systems. In *Global Warming of 1.5°C. An IPCC special report on the impacts of global warming of 1.5°C above pre-industrial levels and related global greenhouse gas emission pathways, in the context of strengthening the global response to the threat of climate change, sustainable development, and efforts to eradicate poverty*. Retrieved from https://www.ipcc.ch/sr15/chapter/chapter-3/

Holland, G. (2008). A revised hurricane pressure–wind model. *Monthly Weather Review*, *136*(9), 3432–3445. https://doi.org/10.1175/2008MWR2395.1

Hsiang, S., & Jina, A. (2014). The causal effect of environmental catastrophe on long-run economic growth: Evidence from 6,700 cyclones. *National Bureau of Economic Research*. https://doi.org/10.3386/w20352

Huang, S., Kumar, R., Flörke, M., Yang, T., Hundecha, Y., Kraft, P., et al. (2017). Evaluation of an ensemble of regional hydrological models in 12 large-scale river basins worldwide. *Climatic Change*, *141*(3), 381–397. https://doi.org/10.1007/s10584-016-1841-8

IDMC (2020). Global report on internal displacement 2020. Retrieved from https://www.internal-displacement.org/global-report/grid2020/

IMF (2019). World economic outlook database, April 2019. Retrieved from https://www.imf.org/external/pubs/ft/weo/2019/01/weodata/index.aspx (Accessed on 13 February 2020)

Im, E.-S., Pal, J. S., & Eltahir, E. A. B. (2017). Deadly heat waves projected in the densely populated agricultural regions of South Asia. *Science Advances*, *3*(8), e1603322. https://doi.org/10.1126/sciadv.1603322

Jolly, W. M., Cochrane, M. A., Freeborn, P. H., Holden, Z. A., Brown, T. J., Williamson, G. J., & Bowman, D. M. J. S. (2015). Climate-induced variations in global wildfire danger from 1979 to 2013. *Nature Communications*, *6*, 7537. https://doi.org/10.1038/ncomms8537

Kamali, B., Abbaspour, K. C., Lehmann, A., Wehrli, B., & Yang, H. (2018). Spatial assessment of maize physical drought vulnerability in sub-Saharan Africa: Linking drought exposure with crop failure. *Environmental Research Letters*, *13*(7), 074010. https://doi.org/10.1088/1748-9326/aacb37

King, A. D., & Harrington, L. J. (2018). The inequality of climate change From 1.5 to 2°C of global warming. *Geophysical Research Letters*, *45*, 5030–5033. https://doi.org/10.1029/2018GL078430

Klein Goldewijk, K., Beusen, A., Doelman, J., & Stehfest, E. (2017). Anthropogenic land use estimates for the Holocene—HYDE 3.2. *Earth System Science Data*, *9*(2), 927–953. https://doi.org/10.5194/essd-9-927-2017

Knox, J., Daccache, A., Hess, T., & Haro, D. (2016). Meta-analysis of climate impacts and uncertainty on crop yields in Europe. *Environmental Research Letters*, *11*(11), 113004. https://doi.org/10.1088/1748-9326/11/11/113004

Knox, J., Hess, T., Daccache, A., & Wheeler, T. (2012). Climate change impacts on crop productivity in Africa and South Asia. *Environmental Research Letters*, *7*(3), 034032. https://doi.org/10.1088/1748-9326/7/3/034032

Knutson, T. R., McBride, J. L., Chan, J., Emanuel, K., Holland, G., Landsea, C., et al. (2010). Tropical cyclones and climate change. *Nature Geoscience*, *3*, 157. https://doi.org/10.1038/ngeo779

Knutson, T. R., & Tuleya, R. E. (2004). Impact of CO_2-induced warming on simulated hurricane intensity and precipitation: Sensitivity to the choice of climate model and convective parameterization. *Journal of Climate*, *17*(18), 3477–3495. https://doi.org/10.1175/1520-0442(2004)017<3477:IOCWOS>2.0.CO;2

Koirala, S., Yeh, P. J.-F., Hirabayashi, Y., Kanae, S., & Oki, T. (2014). Global-scale land surface hydrologic modeling with the representation of water table dynamics. *Journal of Geophysical Research: Atmospheres*, *119*, 75–89. https://doi.org/10.1002/2013JD020398

Konovalov, I. B., Beekmann, M., Kuznetsova, I. N., Yurova, A., & Zvyagintsev, A. M. (2011). Atmospheric impacts of the 2010 Russian wildfires: Integrating modelling and measurements of an extreme air pollution episode in the Moscow region. *Atmospheric Chemistry and Physics*, *11*(19), 10,031–10,056. https://doi.org/10.5194/acp-11-10031-2011

Kousky, C. (2014). Informing climate adaptation: A review of the economic costs of natural disasters. *Energy Economics*, *46*, 576–592. https://doi.org/10.1016/j.eneco.2013.09.029

Lange, S. (2017). ISIMIP2b bias-correction code. https://doi.org/10.5281/zenodo.1069050

Lange, S. (2018). Bias correction of surface downwelling longwave and shortwave radiation for the EWEMBI dataset. *Earth System Dynamics*, *9*(2), 627–645. https://doi.org/10.5194/esd-9-627-2018

Lange, S., Rockel, B., Volkholz, J., & Bookhagen, B. (2015). Regional climate model sensitivities to parametrizations of convection and non-precipitating subgrid-scale clouds over South America. *Climate Dynamics*, *44*(9-10), 2839–2857. https://doi.org/10.1007/s00382-014-2199-0

Lee, C.-Y., Camargo, S. J., Sobel, A. H., & Tippett, M. K. (2020). Statistical-dynamical downscaling projections of tropical cyclone activity in a warming climate: Two diverging genesis scenarios. *Journal of Climate*, *33*, 4815–4834. https://doi.org/10.1175/JCLI-D-19-0452.1

Lehmann, J., Coumou, D., & Frieler, K. (2015). Increased record-breaking precipitation events under global warming. *Climatic Change*, *132*(4), 501–515. https://doi.org/10.1007/s10584-015-1434-y

Lehner, F., Coats, S., Stocker, T. F., Pendergrass, A. G., Sanderson, B. M., Raible, C. C., & Smerdon, J. E. (2017). Projected drought risk in 1.5°C and 2°C warmer climates. *Geophysical Research Letters*, *44*, 7419–7428. https://doi.org/10.1002/2017GL074117

Lobell, D. B., Schlenker, W., & Costa-Roberts, J. (2011). Climate trends and global crop production since 1980. *Science*, *333*, 616–620. https://doi.org/10.1126/science.1204531

Mahlstein, I., Knutti, R., Solomon, S., & Portmann, R. W. (2011). Early onset of significant local warming in low latitude countries. *Environmental Research Letters*, *6*(3), 034009. https://doi.org/10.1088/1748-9326/6/3/034009

Masterton, J. M., & Richardson, F. A. (1979). *Humidex: A method of quantifying human discomfort due to excessive heat and humidity*. Environment Canada, Atmospheric Environment. Retrieved from https://books.google.de/books?id=2uH5ygAACAAJ

Mehran, A., Mazdiyasni, O., & AghaKouchak, A. (2015). A hybrid framework for assessing socioeconomic drought: Linking climate variability, local resilience, and demand. *Journal of Geophysical Research: Atmospheres*, *120*, 7520–7533. https://doi.org/10.1002/2015JD023147

Mendelsohn, R. O. (2006). A critique of the stern report. Is there a case for aggressive, near-term mitigation of greenhouse gases? *Regulation*, *Winter 2006–2007* (pp. 42–46). Retrieved from http://heinonline.org/HOL/LandingPage?handle=hein.journals/rcatorbg29&div=58&id=&page=

Mendelsohn, R. O., Dinar, A., & Williams, L. (2006). The distributional impact of climate change on rich and poor countries. *Environment and Development Economics*, *11*(2), 159–178. https://doi.org/10.1017/s1355770x05002755

Mendelsohn, R. O., Emanuel, K., Chonabayashi, S., & Bakkensen, L. (2012). The impact of climate change on global tropical cyclone damage. *Nature Climate Change*, *2*(3), 205–209. https://doi.org/10.1038/nclimate1357

Milly, P. C. D., & Dunne, K. A. (2017). A hydrologic drying bias in water-resource impact analyses of anthropogenic climate change. *JAWRA Journal of the American Water Resources Association*, *53*(4), 822–838. https://doi.org/10.1111/1752-1688.12538

Minoli, S., Müller, C., Elliott, J., Ruane, A. C., Jägermeyr, J., Zabel, F., et al. (2019). Global response patterns of major rainfed crops to adaptation by maintaining current growing periods and irrigation. *Earth's Future*, *7*, 1464–1480. https://doi.org/10.1029/2018EF001130

Müller, C., Elliott, J., Chryssanthacopoulos, J., Arneth, A., Balkovic, J., Ciais, P., et al. (2017). Global gridded crop model evaluation: Benchmarking, skills, deficiencies and implications. *Geoscientific Model Development*, *10*(4), 1403–1422. https://doi.org/10.5194/gmd-10-1403-2017

Munich RE (2020). NatCatSERVICE analysis tool. Retrieved from https://natcatservice.munichre.com/

Nyabeze, W. R. (2004). Estimating and interpreting hydrological drought indices using a selected catchment in Zimbabwe. *Physics and Chemistry of the Earth, Parts A/B/C*, *29*(15), 1173–1180. https://doi.org/10.1016/j.pce.2004.09.018

Oleson, K. W., Bonan, G. B., Feddema, J., & Jackson, T. (2011). An examination of urban heat island characteristics in a global climate model. *International Journal of Climatology*, *31*(12), 1848–1865. https://doi.org/10.1002/joc.2201

Oppenheimer, M., Campos, M., Warren, R., Birkmann, J., Luber, G., O'Neill, B., & Takahashi, K. (2014). Emergent risks and key vulnerabilities. In Field, C. B. et al. (Eds.), *Climate change 2014: Impacts, adaptation, and vulnerability. Part A: Global and sectoral aspects. Contribution of Working Group II to the fifth assessment report of the Intergovernmental Panel on Climate Change* (pp. 1039–1099). Cambridge, United Kingdom and New York, NY, USA: Cambridge University Press.

Ostberg, S., Schewe, J., Childers, K., & Frieler, K. (2018). Changes in crop yields and their variability at different levels of global warming. *Earth System Dynamics*, *9*(2), 479–496. https://doi.org/10.5194/esd-9-479-2018

Pappenberger, F., Dutra, E., Wetterhall, F., & Cloke, H. L. (2012). Deriving global flood hazard maps of fluvial floods through a physical model cascade. *Hydrology and Earth System Sciences*, *16*(11), 4143–4156. https://doi.org/10.5194/hess-16-4143-2012

Patricola, C. M., & Wehner, M. F. (2018). Anthropogenic influences on major tropical cyclone events. *Nature*, *563*(7731), 339–346. https://doi.org/10.1038/s41586-018-0673-2

Pechony, O., & Shindell, D. T. (2010). Driving forces of global wildfires over the past millennium and the forthcoming century. *Proceedings of the National Academy of Sciences*, *107*(45), 19,167–19,170. https://doi.org/10.1073/pnas.1003669107

Peduzzi, P., Chatenoux, B., Dao, H., De Bono, A., Herold, C., Kossin, J., et al. (2012). Global trends in tropical cyclone risk. *Nature Climate Change*, *2*(4), 289–294. https://doi.org/10.1038/nclimate1410

Perkins, S. E. (2015). A review on the scientific understanding of heatwaves—Their measurement, driving mechanisms, and changes at the global scale. *Atmospheric Research*, *164–165*, 242–267. https://doi.org/10.1016/j.atmosres.2015.05.014

Pielke, R. A. (2007). Future economic damage from tropical cyclones: Sensitivities to societal and climate changes. *Philosophical Transactions of the Royal Society A: Mathematical, Physical and Engineering Sciences*, *365*(1860), 2717–2729. https://doi.org/10.1098/rsta.2007.2086

Piontek, F., Müller, C., Pugh, T. A. M., Clark, D. B., Deryng, D., Elliott, J., et al. (2014). Multisectoral climate impact hotspots in a warming world. *Proceedings of the National Academy of Sciences*, *111*(9), 3233–3238. https://doi.org/10.1073/pnas.1222471110

Prudhomme, C., Giuntoli, I., Robinson, E. L., Clark, D. B., Arnell, N. W., Dankers, R., et al. (2014). Hydrological droughts in the 21st century, hotspots and uncertainties from a global multimodel ensemble experiment. *Proceedings of the National Academy of Sciences*, *111*(9), 3262–3267. https://doi.org/10.1073/pnas.1222473110

Puma, M. J., Bose, S., Chon, S. Y., & Cook, B. I. (2015). Assessing the evolving fragility of the global food system. *Environmental Research Letters*, *10*(2), 024007. https://doi.org/10.1088/1748-9326/10/2/024007

Randall, D., Khairoutdinov, M., Arakawa, A., & Grabowski, W. (2003). Breaking the cloud parameterization deadlock. *Bulletin of the American Meteorological Society*, *84*(11), 1547–1564. https://doi.org/10.1175/BAMS-84-11-1547

Reyer, C. P. O., Chang, J., Chen, M., Forrest, M., François, L., Henrot, A.-J., et al. (2019). ISIMIP2b simulation data from biomes sector. GFZ Data Services, 10.5880/PIK.2019.012.
Reyer, C. P. O., Otto, I. M., Adams, S., Albrecht, T., Baarsch, F., Cartsburg, M., et al. (2017). Climate change impacts in Central Asia and their implications for development. *Regional Environmental Change*, *17*(6), 1639–1650. https://doi.org/10.1007/s10113-015-0893-z
Rosenzweig, C., Arnell, N. W., Ebi, K. L., Lotze-Campen, H., Raes, F., Rapley, C., et al. (2017). Assessing inter-sectoral climate change risks: The role of ISIMIP. *Environmental Research Letters*, *12*(1), 010301. https://doi.org/10.1088/1748-9326/12/1/010301
Rosenzweig, C., Elliott, J., Deryng, D., Ruane, A. C., Müller, C., Arneth, A., et al. (2014). Assessing agricultural risks of climate change in the 21st century in a global gridded crop model intercomparison. *Proceedings of the National Academy of Sciences*, *111*(9), 3268–3273. https://doi.org/10.1073/pnas.1222463110
Russo, S., Sillmann, J., & Fischer, E. M. (2015). Top ten European heatwaves since 1950 and their occurrence in the coming decades. *Environmental Research Letters*, *10*(12), 124003. https://doi.org/10.1088/1748-9326/10/12/124003
Russo, S., Sillmann, J., & Sterl, A. (2017). Humid heat waves at different warming levels. *Scientific Reports*, *7*(1), 7477. https://doi.org/10.1038/s41598-017-07536-7
Samaniego, L., Kumar, R., Breuer, L., Chamorro, A., Flörke, M., Pechlivanidis, I. G., et al. (2017). Propagation of forcing and model uncertainties on to hydrological drought characteristics in a multi-model century-long experiment in large river basins. *Climatic Change*, *141*(3), 435–449. https://doi.org/10.1007/s10584-016-1778-y
Schauberger, B., Archontoulis, S., Arneth, A., Balkovic, J., Ciais, P., Deryng, D., et al. (2017). Consistent negative response of us crops to high temperatures in observations and crop models. *Nature Communications*, *8*, 13931. https://doi.org/10.1038/ncomms13931
Schelling, T. C. (1992). Some economics of global warming. *The American Economic Review*, *82*(1), 1–14.
Schewe, J., Gosling, S. N., Reyer, C., Zhao, F., Ciais, P., Elliott, J., et al. (2019). State-of-the-art global models underestimate impacts from climate extremes. *Nature Communications*, *10*(1), 1005. https://doi.org/10.1038/s41467-019-08745-6
Schleussner, C.-F., Deryng, D., Müller, C., Elliott, J., Saeed, F., Folberth, C., et al. (2018). Crop productivity changes in 1.5 °C and 2 °C worlds under climate sensitivity uncertainty. *Environmental Research Letters*, *13*(6), 064007. https://doi.org/10.1088/1748-9326/aab63b
Scussolini, P., Aerts, J. C. J. H., Jongman, B., Bouwer, L. M., Winsemius, H. C., de Moel, H., & Ward, P. J. (2016). FLOPROS: An evolving global database of flood protection standards. *Natural Hazards and Earth System Sciences*, *16*(5), 1049–1061. https://doi.org/10.5194/nhess-16-1049-2016
Seneviratne, S. I., Corti, T., Davin, E. L., Hirschi, M., Jaeger, E. B., Lehner, I., et al. (2010). Investigating soil moisture-climate interactions in a changing climate: A review. *Earth-Science Reviews*, *99*(3), 125–161. https://doi.org/10.1016/j.earscirev.2010.02.004
Sheffield, J., & Wood, E. F. (2008). Projected changes in drought occurrence under future global warming from multi-model, multi-scenario, IPCC AR4 simulations. *Climate Dynamics*, *31*(1), 79–105. https://doi.org/10.1007/s00382-007-0340-z
Sherwood, S. C., & Huber, M. (2010). An adaptability limit to climate change due to heat stress. *Proceedings of the National Academy of Sciences*, *107*(21), 9552–9555. https://doi.org/10.1073/pnas.0913352107
Sobel, A. H., Camargo, S. J., Hall, T. M., Lee, C.-Y., Tippett, M. K., & Wing, A. A. (2016). Human influence on tropical cyclone intensity. *Science*, *353*(6296), 242–246. https://doi.org/10.1126/science.aaf6574
Stahl, K. (2001). Hydrological drought—A study across Europe (Ph.D. Thesis). Freiburg, Germany: Albert-Ludwigs-Universität.
Staudinger, M., Stahl, K., Seibert, J., Clark, M. P., & Tallaksen, L. M. (2011). Comparison of hydrological model structures based on recession and low flow simulations. *Hydrology and Earth System Sciences*, *15*(11), 3447–3459. https://doi.org/10.5194/hess-15-3447-2011
Stocker, T. F., Qin, D., Plattner, G. K., Tignor, M., Allen, S. K., Boschung, J., et al. (2013). *Climate Change 2013: The physical science basis. Contribution of Working Group I to the fifth assessment report of the Intergovernmental Panel on Climate Change* (pp. 1–27). Cambridge, UK and New York, NY, USA: Cambridge University Press.
Stocker, B. D., Zscheischler, J., Keenan, T. F., Prentice, I. C., Seneviratne, S. I., & Peñuelas, J. (2019). Drought impacts on terrestrial primary production underestimated by satellite monitoring. *Nature Geoscience*, *12*(4), 264–270. https://doi.org/10.1038/s41561-019-0318-6
Tao, F., Rötter, R. P., Palosuo, T., Gregorio Hernández Díaz-Ambrona, C., Mínguez, M. I., Semenov, M. A., et al. (2018). Contribution of crop model structure, parameters and climate projections to uncertainty in climate change impact assessments. *Global Change Biology*, *24*(3), 1291–1307. https://doi.org/10.1111/gcb.14019
Taylor, K. E., Stouffer, R. J., & Meehl, G. A. (2011). An overview of CMIP5 and the experiment design. *Bulletin of the American Meteorological Society*, *93*(4), 485–498. https://doi.org/10.1175/BAMS-D-11-00094.1
Tol, R. S. J. (2018). The economic impacts of climate change. *Review of Environmental Economics and Policy*, *12*(1), 4–25. https://doi.org/10.1093/reep/rex027
Trenberth, K. E., Fasullo, J. T., & Shepherd, T. G. (2015). Attribution of climate extreme events. *Nature Climate Change*, *5*(8), 725–730. https://doi.org/10.1038/nclimate2657
Turco, M., Rosa-Cánovas, J. J., Bedia, J., Jerez, S., Montávez, J. P., Llasat, M. C., & Provenzale, A. (2018). Exacerbated fires in Mediterranean Europe due to anthropogenic warming projected with non-stationary climate-fire models. *Nature Communications*, *9*(1), 3821. https://doi.org/10.1038/s41467-018-06358-z
UNFCCC (2016). Adoption of the Paris Agreement, decision 1/CP.21 of FCCC/CP/2015/10/Add.1. https://unfccc.int/resource/docs/2015/cop21/eng/10a01.pdf, Access date: 27 September 2019.
Van Loon, A. F. (2015). Hydrological drought explained. *Wiley Interdisciplinary Reviews: Water*, *2*(4), 359–392. https://doi.org/10.1002/wat2.1085
van der Werf, G. R., Randerson, J. T., Giglio, L., van Leeuwen, T. T., Chen, Y., Rogers, B. M., et al. (2017). Global fire emissions estimates during 1997–2016. *Earth System Science Data*, *9*(2), 697–720. https://doi.org/10.5194/essd-9-697-2017
Vecchi, G. A., Delworth, T. L., Murakami, H., Underwood, S. D., Wittenberg, A. T., Zeng, F., et al. (2019). Tropical cyclone sensitivities to CO_2 doubling: Roles of atmospheric resolution, synoptic variability and background climate changes. *Climate Dynamics*, *53*(9), 5999–6033. https://doi.org/10.1007/s00382-019-04913-y
Velázquez, J. A., Schmid, J., Ricard, S., Muerth, M. J., Gauvin St-Denis, B., Minville, M., et al. (2013). An ensemble approach to assess hydrological models' contribution to uncertainties in the analysis of climate change impact on water resources. *Hydrology and Earth System Sciences*, *17*(2), 565–578. https://doi.org/10.5194/hess-17-565-2013
Veldkamp, T. I. E., Wada, Y., Aerts, J. C. J. H., Döll, P., Gosling, S. N., Liu, J., et al. (2017). Water scarcity hotspots travel downstream due to human interventions in the 20th and 21st century. *Nature Communications*, *8*, 15697. https://doi.org/10.1038/ncomms15697
Vetter, T., Reinhardt, J., Flörke, M., van Griensven, A., Hattermann, F., Huang, S., et al. (2017). Evaluation of sources of uncertainty in projected hydrological changes under climate change in 12 large-scale river basins. *Climatic Change*, *141*(3), 419–433. https://doi.org/10.1007/s10584-016-1794-y

Vidal, J.-P., Martin, E., Franchistéguy, L., Habets, F., Soubeyroux, J.-M., Blanchard, M., & Baillon, M. (2010). Multilevel and multiscale drought reanalysis over France with the Safran-Isba-Modcou hydrometeorological suite. *Hydrology and Earth System Sciences*, *14*(3), 459–478. https://doi.org/10.5194/hess-14-459-2010

Walsh, K. J. E., McBride, J. L., Klotzbach, P. J., Balachandran, S., Camargo, S. J., Holland, G., et al. (2016). Tropical cyclones and climate change. *Wiley Interdisciplinary Reviews: Climate Change*, *7*(1), 65–89. https://doi.org/10.1002/wcc.371

Webber, H., Lischeid, G., Sommer, M., Finger, R., Nendel, C., Gaiser, T., & Ewert, F. (2020). No perfect storm for crop yield failure in Germany. *Environmental Research Letters*, *15*, 104012. https://doi.org/10.1088/1748-9326/aba2a4

Wehner, M. F., Reed, K. A., Loring, B., Stone, D., & Krishnan, H. (2018). Changes in tropical cyclones under stabilized 1.5 and 2.0°C global warming scenarios as simulated by the Community Atmospheric Model under the HAPPI protocols. *Earth System Dynamics*, *9*(1), 187–195. https://doi.org/10.5194/esd-9-187-2018

Winsemius, H. C., Van Beek, L. P. H., Jongman, B., Ward, P. J., & Bouwman, A. (2013). A framework for global river flood risk assessments. *Hydrology and Earth System Sciences*, *17*(5), 1871–1892. https://doi.org/10.5194/hess-17-1871-2013

Wu, M., Knorr, W., Thonicke, K., Schurgers, G., Camia, A., & Arneth, A. (2015). Sensitivity of burned area in Europe to climate change, atmospheric CO_2 levels, and demography: A comparison of two fire-vegetation models. *Journal of Geophysical Research: Biogeosciences*, *120*, 2256–2272. https://doi.org/10.1002/2015JG003036

Yamazaki, D., de Almeida, G. A. M., & Bates, P. D. (2013). Improving computational efficiency in global river models by implementing the local inertial flow equation and a vector-based river network map. *Water Resources Research*, *49*, 7221–7235. https://doi.org/10.1002/wrcr.20552

Yamazaki, D., Kanae, S., Kim, H., & Oki, T. (2011). A physically based description of floodplain inundation dynamics in a global river routing model. *Water Resources Research*, *47*, W04501. https://doi.org/10.1029/2010WR009726

Yang, J., Tian, H., Tao, B., Ren, W., Kush, J., Liu, Y., & Wang, Y. (2014). Spatial and temporal patterns of global burned area in response to anthropogenic and environmental factors: Reconstructing global fire history for the 20th and early 21st centuries. *Journal of Geophysical Research: Biogeosciences*, *119*, 249–263. https://doi.org/10.1002/2013JG002532

Zhao, F., Veldkamp, T. I. E., Frieler, K., Schewe, J., Ostberg, S., Willner, S., et al. (2017). The critical role of the routing scheme in simulating peak river discharge in global hydrological models. *Environmental Research Letters*, *12*(7), 075003. https://doi.org/10.1088/1748-9326/aa7250

References From the Supporting Information

Best, M. J., Pryor, M., Clark, D. B., Rooney, G. G., Essery, R. L. H., Ménard, C. B., et al. (2011). The Joint UK Land Environment Simulator (JULES), model description—Part 1: Energy and water fluxes. *Geoscientific Model Development*, *4*, 677–699. https://doi.org/10.5194/gmd-4-677-2011

Bondeau, A., Smith, P. C., Zaehle, S., Schaphoff, S., Lucht, W., Cramer, W., et al. (2007). Modelling the role of agriculture for the 20th century global terrestrial carbon balance. *Global Change Biology*, *13*(3), 679–706. https://doi.org/10.1111/j.1365-2486.2006.01305.x

CCOHS (2017). Humidex Rating and Work. Retrieved from https://www.ccohs.ca/oshanswers/physagents/humidex.html (Access date: 27 October 2017).

Dury, M., Hambuckers, A., Warnant, P., Henrot, A., Favre, E., Ouberdous, M., & Frančois, L. (2011). Responses of European forest ecosystems to 21st century climate: Assessing changes in interannual variability and fire intensity. *iForest Biogeosciences and Forestry*, *4*, 82–99. https://doi.org/10.3832/ifor0572-004

Elliott, J., Müller, C., Deryng, D., Chryssanthacopoulos, J., Boote, K. J., Büchner, M., et al. (2015). The Global Gridded Crop Model Intercomparison: Data and modeling protocols for Phase 1 (v1.0). *Geoscientific Model Development*, *8*(2), 261–277. https://doi.org/10.5194/gmd-8-261-2015

Folberth, C., Elliott, J., Müller, C., Balkovic, J., Chryssanthacopoulos, J., Izaurralde, R. C., et al. (2016). Uncertainties in global crop model frameworks: Effects of cultivar distribution, crop management and soil handling on crop yield estimates. *Biogeosciences Discussions*, *2016*, 1–30. https://doi.org/10.5194/bg-2016-527

Folberth, C., Gaiser, T., Abbaspour, K. C., Schulin, R., & Yang, H. (2012). Regionalization of a large-scale crop growth model for sub-Saharan Africa: Model setup, evaluation, and estimation of maize yields. *Agriculture, Ecosystems & Environment*, *151*, 21–33. https://doi.org/10.1016/j.agee.2012.01.026

Frank, W. M., & Young, G. S. (2007). The interannual variability of tropical cyclones. *Monthly Weather Review*, *135*(10), 3587–3598. https://doi.org/10.1175/MWR3435.1

Giglio, L., Randerson, J. T., & van der Werf, G. R. (2013). Analysis of daily, monthly, and annual burned area using the fourth-generation global fire emissions database (GFED4). *Journal of Geophysical Research: Biogeosciences*, *118*, 317–328. https://doi.org/10.1002/jgrg.20042

Giglio, L., Randerson, J. T., van der Werf, G. R., Kasibhatla, P. S., Collatz, G. J., Morton, D. C., & DeFries, R. S. (2010). Assessing variability and long-term trends in burned area by merging multiple satellite fire products. *Biogeosciences*, *7*(3), 1171–1186. https://doi.org/10.5194/bg-7-1171-2010

Guimberteau, M., Ducharne, A., Ciais, P., Boisier, J. P., Peng, S., De Weirdt, M., & Verbeeck, H. (2014). Testing conceptual and physically based soil hydrology schemes against observations for the Amazon Basin. *Geoscientific Model Development*, *7*(3), 1115–1136. https://doi.org/10.5194/gmd-7-1115-2014

Hagemann, S., & Dümenil Gates, L. (2003). Improving a subgrid runoff parameterization scheme for climate models by the use of high resolution data derived from satellite observations. *Climate Dynamics*, *21*(3–4), 349–359. https://doi.org/10.1007/s00382-003-0349-x

Hanasaki, N., Yoshikawa, S., Pokhrel, Y., & Kanae, S. (2018). A global hydrological simulation to specify the sources of water used by humans. *Hydrology and Earth System Sciences*, *22*(1), 789–817. https://doi.org/10.5194/hess-22-789-2018

Hosking, J., & Wallis, J. (2005). *Regional frequency analysis: An approach based on L-moments*: Cambridge University Press.

Ito, A., & Inatomi, M. (2012). Water-use efficiency of the terrestrial biosphere: A model analysis focusing on interactions between the global carbon and water cycles. *Journal of Hydrometeorology*, *13*(2), 681–694. https://doi.org/10.1175/JHM-D-10-05034.1

Ito, A., & Oikawa, T. (2002). A simulation model of the carbon cycle in land ecosystems (Sim-CYCLE): A description based on dry-matter production theory and plot-scale validation. *Ecological Modelling*, *151*(2), 143–176. https://doi.org/10.1016/S0304-3800(01)00473-2

Jenkinson, A. F. (1955). The frequency distribution of the annual maximum (or minimum) values of meteorological elements. *Quarterly Journal of the Royal Meteorological Society*, *81*(348), 158–171. https://doi.org/10.1002/qj.49708134804

Kato, E., Kinoshita, T., Ito, A., Kawamiya, M., & Yamagata, Y. (2013). Evaluation of spatially explicit emission scenario of land-use change and biomass burning using a process-based biogeochemical model. *Journal of Land Use Science*, *8*(1), 104–122. https://doi.org/10.1080/1747423X.2011.628705

Lawrence, D. M., Oleson, K. W., Flanner, M. G., Thornton, P. E., Swenson, S. C., Lawrence, P. J., et al. (2011). Parameterization improvements and functional and structural advances in version 4 of the Community Land Model. *Journal of Advances in Modeling Earth Systems*, *3*, M03001. https://doi.org/10.1029/2011MS00045

Liu, W., Yang, H., Folberth, C., Wang, X., Luo, Q., & Schulin, R. (2016). Global investigation of impacts of PET methods on simulating crop-water relations for maize. *Agricultural and Forest Meteorology*, *221*, 164–175. https://doi.org/10.1016/j.agrformet.2016.02.017

Liu, W., Yang, H., Liu, J., Azevedo, L. B., Wang, X., Xu, Z., et al. (2016). Global assessment of nitrogen losses and trade-offs with yields from major crop cultivations. *Science of The Total Environment*, *572*, 526–537. https://doi.org/10.1016/j.scitotenv.2016.08.093

Mouillot, F., & Field, C. B. (2005). Fire history and the global carbon budget: A 1° × 1° fire history reconstruction for the 20th century. *Global Change Biology*, *11*(3), 398–420. https://doi.org/10.1111/j.1365-2486.2005.00920.x

Müller Schmied, H., Adam, L., Eisner, S., Fink, G., Flörke, M., Kim, H., et al. (2016). Variations of global and continental water balance components as impacted by climate forcing uncertainty and human water use. *Hydrology and Earth System Sciences*, *20*(7), 2877–2898. https://doi.org/10.5194/hess-20-2877-2016

Müller Schmied, H., Eisner, S., Franz, D., Wattenbach, M., Portmann, F. T., Flörke, M., & Döll, P. (2014). Sensitivity of simulated global-scale freshwater fluxes and storages to input data, hydrological model structure, human water use and calibration. *Hydrology and Earth System Sciences*, *18*(9), 3511–3538. https://doi.org/10.5194/hess-18-3511-2014

Oleson, K. W., Lawrence, D. M., Bonan, G. B., Drewniak, B., Huang, M., Koven, C. D., et al. (2013). Technical description of version 4.5 of the Community Land Model (CLM), *NCAR/TN-503+STR*. https://doi.org/10.5065/D6RR1W7M

Papadimitriou, L. V., Koutroulis, A. G., Grillakis, M. G., & Tsanis, I. K. (2017). The effect of GCM biases on global runoff simulations of a land surface model. *Hydrology and Earth System Sciences*, *21*(9), 4379–4401. https://doi.org/10.5194/hess-21-4379-2017

Pierce, L. T. (1934). Diurnal variation in the dew-point temperature at Asheville N. C. *Monthly Weather Review*, *62*(8), 289–293. https://doi.org/10.1175/1520-0493(1934)62<289:DVITDT>2.0.CO;2

Plummer, S. J., Arino, O., Beusen, B., Fierens, F., Heyns, W., Benedetti, R., et al. (2007). An Update on the globcarbon initiative: Multi-sensor estimation of global biophysical products for global terrestrial carbon studies. In *Proceedings of Envisat Symposium 2007, 23–27 April 2007, Montreux, Switzerland*, ESA Communication Production Office, ESTEC.

Rost, S., Gerten, D., Bondeau, A., Lucht, W., Rohwer, J., & Schaphoff, S. (2008). Agricultural green and blue water consumption and its influence on the global water system. *Water Resources Research*, *44*, W09405. https://doi.org/10.1029/2007WR006331

Sacks, W. J., Deryng, D., Foley, J. A., & Ramankutty, N. (2010). Crop planting dates: An analysis of global patterns. *Global Ecology and Biogeography*, *19*(5), 607–620. https://doi.org/10.1111/j.1466-8238.2010.00551.x

Schaphoff, S., Heyder, U., Ostberg, S., Gerten, D., Heinke, J., & Lucht, W. (2013). Contribution of permafrost soils to the global carbon budget. *Environmental Research Letters*, *8*(1), 014026. https://doi.org/10.1088/1748-9326/8/1/014026

Schwartzman, P. D., Michaels, P. J., & Knappenberger, P. C. (1998). Observed changes in the diurnal dewpoint cycles across North America. *Geophysical Research Letters*, *25*(13), 2265–2268. https://doi.org/10.1029/98GL01843

Smith, B., Wårlind, D., Arneth, A., Hickler, T., Leadley, P., Siltberg, J., & Zaehle, S. (2014). Implications of incorporating N cycling and N limitations on primary production in an individual-based dynamic vegetation model. *Biogeosciences*, *11*(7), 2027–2054. https://doi.org/10.5194/bg-11-2027-2014

Stacke, T., & Hagemann, S. (2012). Development and validation of a global dynamical wetlands extent scheme. *Hydrology and Earth System Sciences Discussions*, *9*(1), 405–440. https://doi.org/10.5194/hessd-9-405-2012

Stehfest, E., Heistermann, M., Priess, J. A., Ojima, D. S., & Alcamo, J. (2007). Simulation of global crop production with the ecosystem model DayCent. *Ecological Modelling*, *209*(2), 203–219. https://doi.org/10.1016/j.ecolmodel.2007.06.028

Takata, K., Emori, S., & Watanabe, T. (2003). Development of the minimal advanced treatments of surface interaction and runoff. *Global and Planetary Change*, *38*(1), 209–222. https://doi.org/10.1016/S0921-8181(03)00030-4

Tansey, K., Grégoire, J.-M., Defourny, P., Leigh, R., Pekel, J.-F., van Bogaert, E., & Bartholomé, E. (2008). A new, global, multi-annual (2000–2007) burnt area product at 1 km resolution. *Geophysical Research Letters*, *35*, L01401. https://doi.org/10.1029/2007GL031567

Thonicke, K., Spessa, A., Prentice, I. C., Harrison, S. P., Dong, L., & Carmona-Moreno, C. (2010). The influence of vegetation, fire spread and fire behaviour on biomass burning and trace gas emissions: Results from a process-based model. *Biogeosciences*, *7*(6), 1991–2011. https://doi.org/10.5194/bg-7-1991-2010

Thonicke, K., Venevsky, S., Sitch, S., & Cramer, W. (2001). The role of fire disturbance for global vegetation dynamics: Coupling fire into a Dynamic Global Vegetation Model. *Global Ecology and Biogeography*, *10*(6), 661–677. https://doi.org/10.1046/j.1466-822X.2001.00175.x

Wada, Y., de Graaf, I. E. M., & van Beek, L. P. H. (2016). High-resolution modeling of human and climate impacts on global water resources. *Journal of Advances in Modeling Earth Systems*, *8*, 735–763. https://doi.org/10.1002/2015MS000618

Wada, Y., Wisser, D., & Bierkens, M. F. P. (2014). Global modeling of withdrawal, allocation and consumptive use of surface water and groundwater resources. *Earth System Dynamics*, *5*(1), 15–40. https://doi.org/10.5194/esd-5-15-2014

Ward, P. J., Jongman, B., Kummu, M., Dettinger, M. D., Sperna Weiland, F. C., & Winsemius, H. C. (2014). Strong influence of El Niño Southern Oscillation on flood risk around the world. *Proceedings of the National Academy of Sciences*, *111*(44), 15,659–15,664. https://doi.org/10.1073/pnas.1409822111

Williams, J. (1995). The EPIC model [book section]. In V. P. Singh (Ed.), *Computer models of watershed hydrology* (pp. 909–1000). Littleton, USA: Water Resources Publications.

World Development Indicators (2017). Employment in agriculture (percent of total employment) (modeled ILO estimate). Retrieved from https://data.worldbank.org/indicator/SL.AGR.EMPL.ZS

Yue, C., Ciais, P., Cadule, P., Thonicke, K., Archibald, S., Poulter, B., et al. (2014). Modelling the role of fires in the terrestrial carbon balance by incorporating SPITFIRE into the global vegetation model ORCHIDEE—Part 1: Simulating historical global burned area and fire regimes. *Geoscientific Model Development*, *7*(6), 2747–2767. https://doi.org/10.5194/gmd-7-2747-2014

Yue, C., Ciais, P., Cadule, P., Thonicke, K., & van Leeuwen, T. T. (2015). Modelling the role of fires in the terrestrial carbon balance by incorporating SPITFIRE into the global vegetation model ORCHIDEE Part 2: Carbon emissions and the role of fires in the global carbon balance. *Geoscientific Model Development*, *8*(5), 1321–1338. https://doi.org/10.5194/gmd-8-1321-2015